MASS MANUFACTURE OF MEAs USING HIGH SPEED DEPOSITION PROCESSES

Grant agreement no.: 779591

Start date: 01.01.2018 – **Duration**: 36 months
Project Coordinator: Technische Universität Chemnitz

DELIVERABLE REPORT D2.4

D2.4 – LAYER CHARACTERISATION	
Due Date	31 Dec 2019
Author(s)	ENAS, JMFC, TUC, UNIMORE
Work Package	WP2: Technology proof of concept
Work Package Leader	ENAS
Lead Beneficiary	ENAS
Date released by WP Leader	22-Jun-2021
Date released by Coordinator	28-Jun-2021

DISSEMINATION LEVEL		
PU	*Public*	*X*
PP	*Restricted to other programme participants (including the Commission Services)*	
RE	*Restricted to a group specified by the consortium (including the Commission Services)*	
CO	*Confidential, only for members of the consortium (including the Commission Services)*	

NATURE OF THE DELIVERABLE		
R	*Report*	*X*
P	*Prototype*	
D	*Demonstrator*	
O	*Other*	

D2.4 – SUMMARY	
Keywords	Characterisation, layer thickness, conductivity, roughness, size, accelerated stress test
Full Abstract (Confidential)	The description of a comprehensive suite of tests characterising the deposited layers offline in a morphological way and as well as their ability to perform to the specification under the desired conditions are given. The devices employed, the measurement techniques as well as some sample results are given.
Publishable Abstract (If different from above) *For publication on website*	- same as above -

REVISIONS

Version	Date	Changed by	Comments
0.0	19 Nov 2019	ENAS	Draft
0.1	29 Nov 2019	ENAS	Technologies added
0.2	12 Dec 2019	ENAS	Technology added
0.3	17 Dec 2019	ENAS, NFCT	Review, new section
0.4	20 Dec 2019	UNIMORE	Contents added
0.5	31 Mar 2020	TUC, UNIMORE	Contents added
0.6	06 Apr 2020	TUC; ENAS	Review of text
0.7	30 Apr 2020	UNIMORE	Review, comments addressed
0.8	10 Jun 2020	JM	Content added
0.9	16 Jun 2020	ENAS	consolidation
0.10	02 Jul 2020	JM	Content added
0.11	25 Nov 2020	TUC (ENAS)	Content added
0.12	03 Dec 2020	ENAS	Final draft
0.13	22 Dec 2020	ENAS	Comments added
0.14	30 Apr 2021	TUC, ENAS	Final revision
1.0	28 Jun 2021	TUC, ENAS	Final version

D2.4 – LAYER CHARACTERISATION

TABLE OF CONTENTS

NOMENCLATURE

ALM	Additive Layer Manufacturing
AST	Accelerated Stress Tests
BoL	Beginning of Life
CCM	Catalyst Coated Membrane
CV	Cyclic Voltammetry
ECSA	Electrochemical Active Surface Area
EIS	Electrochemical Impedance Spectroscopy
EoT	End of Test
EoL	End of Life
HFR	High Frequency Resistance
KPI	Key Performance Indicator
MEA	Membrane Electrode Assembly
PTFE	Polytetrafluoroethylene
RH	Relative Humidity
RHE	Reference Hydrogen Electrode
SEM	Scanning Electron Microscope
WP	Work Package

1. INTRODUCTION

This deliverable report describes methodology, machinery as well as achievable measurement results from lab equipment used for characterising deposited layers of CCMs. The main goal of WP2 – *Technology proof of concept* is to deposit layers of catalytic and ionomer inks in laboratory environment by selected printing and coating technologies. These deposited layers require a characterisation about their morphological properties. The results are fed into the development loop of ink composition as well as tweaking the deposition process parameters.

For the production of CCMs an inline process monitoring is desirable. These efforts are done in WP4 – *Manufacturing process design*. The use of offline characterisation technologies at this stage of development is adequate because they usually deliver much more detailed information that can feed into the inline equipment selected for deployment in the pilot MEA manufacturing line.

2. TECHNOLOGIES AVAILABLE AT PARTNER SITES

In this chapter, technologies available and used by the consortium partners are described and assessed. Additionally, some exemplary results are shown for a better understanding.

2.1. EVALUATION OF FOAM FORMATION IN INKS

2.1.1 DESCRIPTION

The inkjet-printing tests for high-volume production have shown foam formation in the employed inks [3]. This phenomenon is due to the fluid-dynamic condition inside to the ink circuit and printhead: air is either entrapped as a result of a less-than-perfect meniscus or already present in the ducts prior to ink loading. Foam is generally considered to be a dispersion of gas in a liquid phase and has macroscopic size beyond the colloidal range. Its life and properties are governed by colloidal and surface forces, and interactions across the film separating individual gas bubbles. Being a non-equilibrium condition, its stability is often quite short, but its lifetime may be long enough to generate problems at the nozzle of the printhead. A possible strategy for the reduction of this issue is to add some anti-foaming agent to the inks. A defoamer or an anti-foaming agent is a chemical additive that reduces and hinders foam formation in a generic liquid. There are various chemical formulations in the market, which can prevent foam formation (anti-foaming) or can destroy it once it has formed (defoamer):

- oil based defoamers;
- powder defoamers;
- water based defoamers;
- silicone based defoamers;
- PG/PGC (polyethylene glycol and polypropylene glycol copolymers) based defoamers;
- alkyl poly acrylates.

In the present case, an ideal additive must meet several requirements, it must:

- be able to reduce the foam already in small doses;
- not reduce the electrochemical activity of the catalyst;
- not reduce the efficiency or durability of the MEA;
- not be corrosive to the inkjet system;
- have low or no toxicity;
- not change the intended interactions between the catalyst layer in liquid and dry form;
- be readily available in the market.

In order to make a well-founded choice of a defoamer, the very first step was to develop a quantitative methodology to measure foam formation, as the open literature currently provides very little reference in that regard. An experimental apparatus was constructed (Figure 1), consisting of a graduated test tube (plastic-made, 10 ml maximum capacity), an injection needle, a flowmeter and a small air compressor.
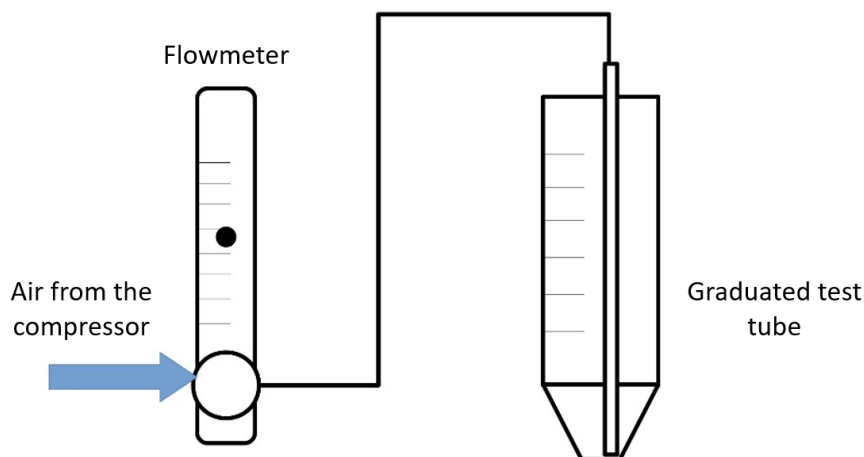
Figure 1 Sketch of the experimental apparatus with main components

The test procedure includes the following steps (Figure 2):
- filling the test tube with a known amount of ink (4 ml, in the tests conducted here);
- allowing the injection needle within the test tube, ensuring that its outlet falls below the ink level;
- connecting the air compressor to the inlet of the injection needle;
- starting the compressor and setting the flow rate thus allowing a controlled amount of air into the ink;
- operating the compressor for a fixed amount (to achieve a given air volume) of time at the same pressure, which generates bubbles within the test tube;
- as air feeding is stopped, measuring the volume of the ink and foam within the test tube;
- the difference between final and initial volume $\Delta V = V_f - V_i$ is an index of foam formation, or – more precisely – of the extent to which the tested ink is prone to foam formation.

The final and initial volume can be measured by taking a photo before and after supplying air inside the test tube, thus generating foam in the ink. Subsequently, by means of an image analysis software or more simply a ruler, the height of the foam with respect to the initial ink level can be measured. In our analysis, the open source ImageJ[1] software – a common image analyser – was used. Since the measurement process is relatively quick, numerous repeats could be performed in order to have a statistically meaningful dataset. The effectiveness of different additives – anti-foaming and defoamers – could be determined quantitatively. Statistical procedures to define the variations as ANOVA (Analysis of Variance) and *post hoc* test were applied with a resulting statistical variance lower than 5 %. Figure 3 shows a visually evident application of the described experiment involving Anode ink 2, with both pre- and post-air supply photos.

---

[1] https://imagej.nih.gov/ij/
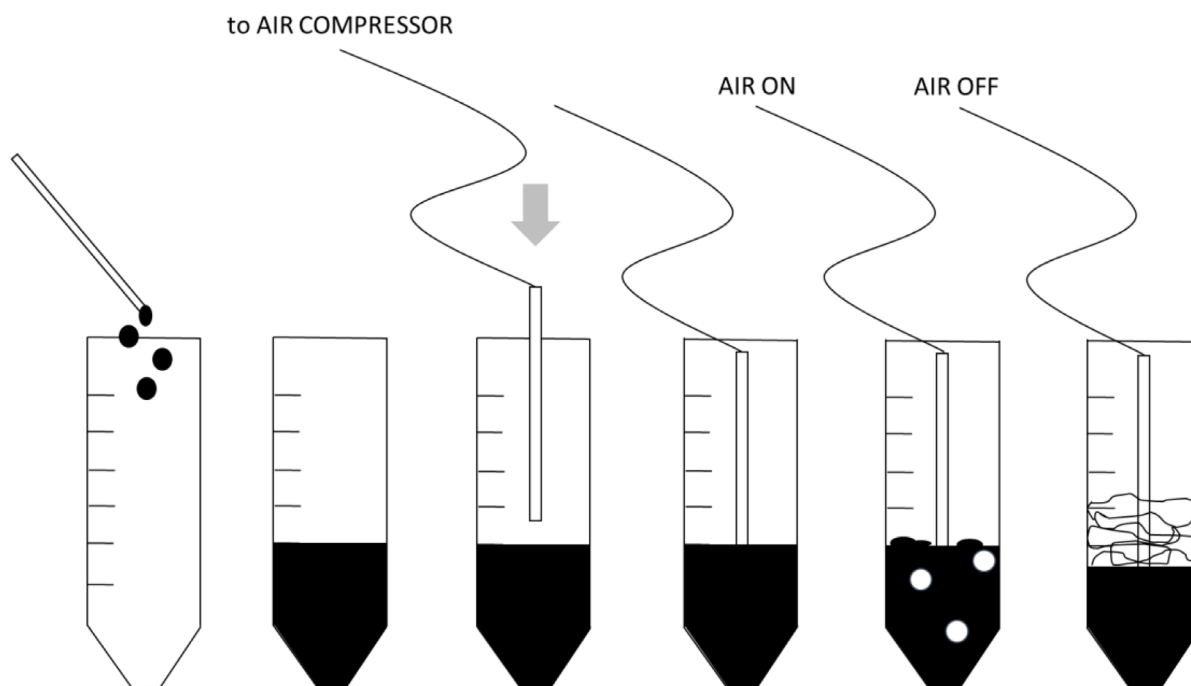
Figure 2 Sketch of the setup and steps of the procedure for evaluating foam formation
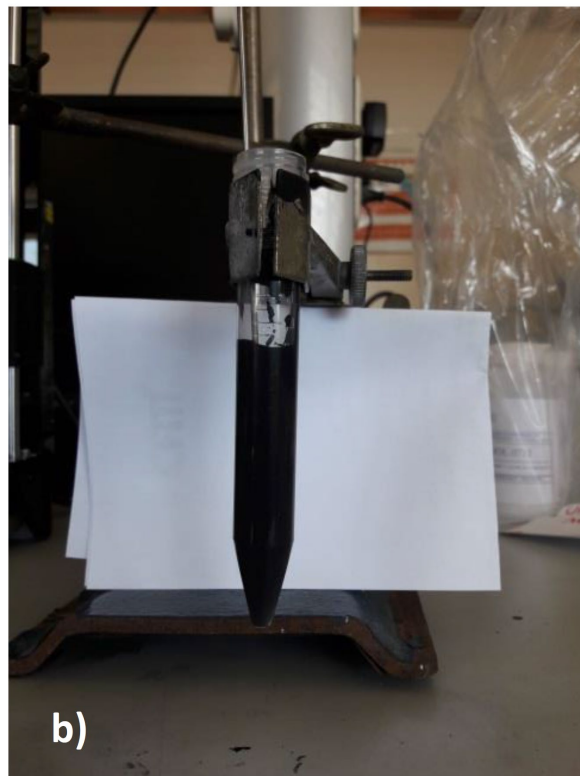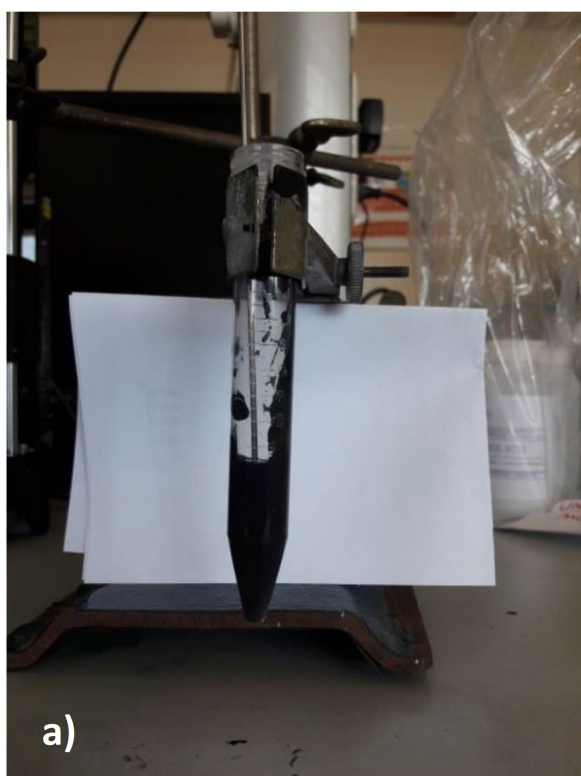
Figure 3 Photos of the test tube filled with pure Anode 2 ink, immediately prior to air feeding (a) and immediately after air-feeding shutoff (b). (source: UNIMORE)

The ΔV resulting from tests on pure Anode 2 ink was 5 ml and was taken as a reference (ΔV_0), since Anode ink 2 was the most prone to foam forming. The ratio between ΔV for any other ink – either endowed with the tested additives or pure – and the reference value ($\Delta V/\Delta V_0$) served as a quantitative measure of the ability of the additive to reduce foam formation, if any, or as an evaluation of the tendency to form foam in pure inks.

2.1.2. MEASUREMENT RESULTS

Several additives were tested, among which some fluorosurfactants – acquired from a chemical manufacturer (Maflon S.p.A.) – under various concentrations (0.05 wt% – 2 wt%) in a mixture with pure Anode 2 ink and ethylene glycol (EG) up to 50 wt%. All the mixtures were prepared by simple magnetic stirring of the sample at least 10 minutes prior to testing. Finally, some defoamers were acquired from a chemical manufacturer (Lamberti S.p.A.), *ad hoc* developed to the purpose:

- non-ionic (Tensiol 0711 and Tensiol 0713);
- silicone-based (Tensiol 0712).

The additive concentration was varied from 0.1 wt% to 2 wt%. The most significant results from the tests by the developed methodology and apparatus are summarised in Figure 4.
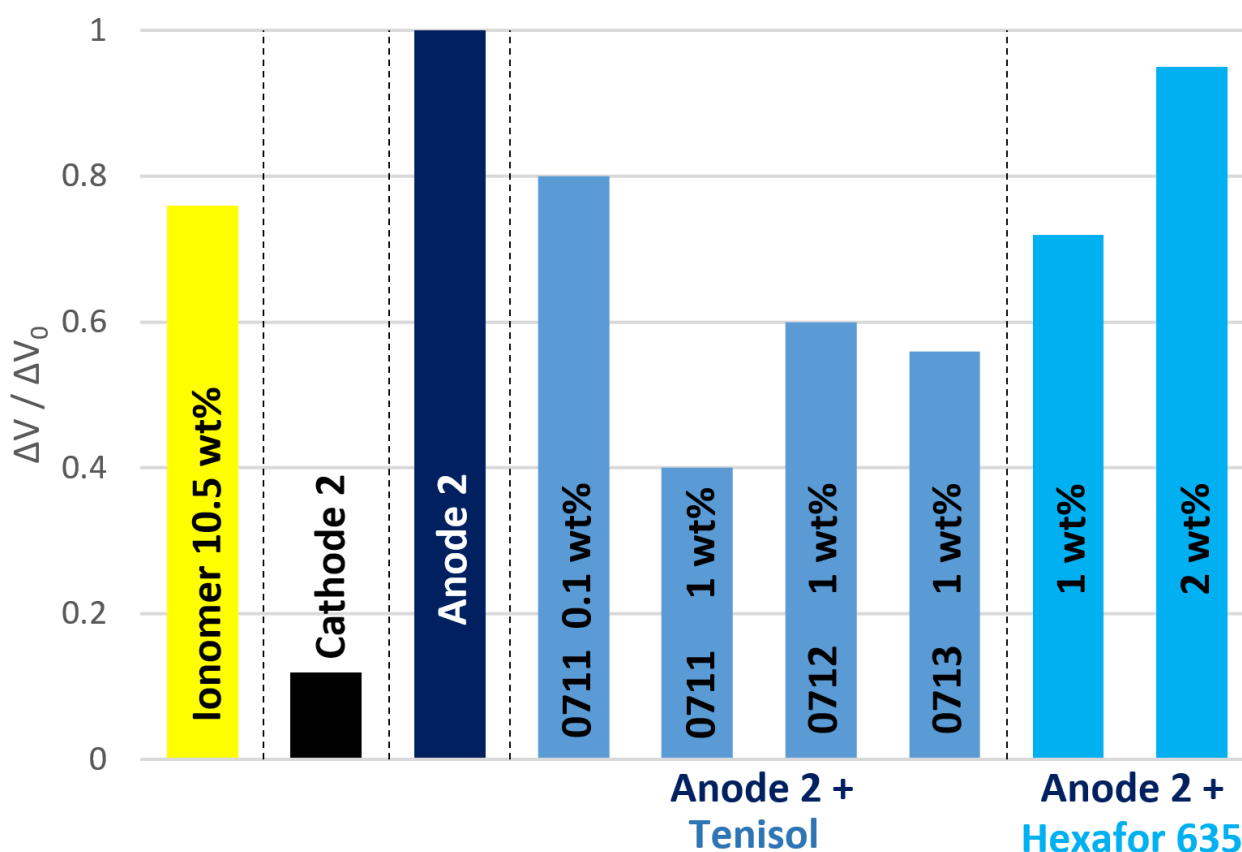
Figure 4. Plot of the experimental results on foam formation against catalyst and ionomer inks

As shown in Figure 4, a perceivable reduction of foam formation, even down to 40 %, was achieved by all the proposed formulations for Anode ink 2, with the higher defoamer concentration (1 wt%) within the mixture being the most effective. Tensiol 0711 (non-ionic) appeared as the most suitable to limit foam formation, whereas silicone-based defoamers – as Tensiol 0712 – and fluorosurfactants – as Hexafor 635 – showed a slightly lower ability to address the problem. In a similar manner to defoamers, fluorosurfactants seem to benefit from a concentration in the order of 1 wt%, whereas

higher concentrations exhibit a reduced anti-foam effect. An attempt was made doubling the concentration to 2 % but it was counterproductive, therefore the recommended intervals by the defoamer producer were followed. On the other hand, Cathode ink 2 did not exhibit a remarkable tendency to form foam (Figure 4), so no use of anti-foam agents or defoamers was deemed necessary. An ionomer solution (10.5 wt% ionomer + 29.75 wt% propan-2-ol + 59.75 wt% water) was also tested; the results are presented in Figure 4. As shown, its tendency to form foam is remarkably smaller than that of pure Anode ink 2, even if most defoamers and fluorosurfactants are capable of achieving even lower foam volumes. However, foam from the ionomer solution exhibited a far shorter lifetime than that associated with catalyst inks: the initial volume was restored in less than 2 min after air feed was shut down, whereas catalyst-ink bubbles persisted significantly even at 5 min after air-feed interruption. This outcome is rather meaningful in high-volume inkjet printing, where air may be entrained into the ink circuit, or in some locations of it.

2.1.3. ASSESSMENT

The proposed experiment does not allow assessing cell performance *per se*; yet, it is an unprecedented approach to evaluate foam formation in inks. It allows assessing printability of a certain ink – only relative to what pertains to foam generation within the ink circuit – against an ink that is either certainly printable (e.g., the developed ionomer solution by the employed fab-scale inkjet printing machine) or certainly not printable (e.g., Anode ink 2 by the employed fab-scale inkjet printing machine). It is important to maintain the same apparatus of the experiment to reproduce the test. It is not possible to compare these results if there are variation like the shape of the graduated test tube or the initial volume of the ink. In addition, another reason to do not exceed with additives and defoamers concentration was to keep as low as possible the presence of foreign elements in the ink.

Figure 5 Usability for ink development in large production requiring ink recirculation

2.2. VISUAL CHARACTERISATION METHODS AND ANALYSIS

Microscopy of samples is a powerful tool that can be used for understanding their structure and the nature of defects. For larger areas even flatbed scanners are of use. In the MAMA-MEA project flatbed scanners are used by TUC, and both optical microscopy and Scanning Electron Microscopy (SEM) have been used in JMFC.

2.2.1. FLATBED SCANNER

2.2.1.1. DESCRIPTION

The in TUC available flatbed scanner is shown in Figure 6. This is a multipurpose device made primarily for copying, printing, and scanning of images in DIN-A4 format. The scanner consists of a flat transparent glass bed under which the charge-coupled device (CCD) sensors, lamp, lenses, filters and also mirrors are fixed. The mechanism of scanning is based on illuminating the white light onto the object with subsequent reading the intensity of the reflecting light. The CCD sensor is used to convert the captured light intensity into the proportional charge values. It is a setup of three sensor lines equipped with a red, green, or blue filter, respectively. The readings from the CCD sensors are

transformed into the digital image in one of the available formats. Maximal resolution for the Triumph-Adler 350ci is 600 dpi.

Figure 6 Flatbed scanner Triumph-Adler (1)

2.2.1.2. MEASUREMENT RESULTS

Clogging of inkjet nozzles during printing catalytic layers is one of the frequently occurring issues. Inkjet printer Fujifilm Dimatix Material Printer 2831 is equipped with fiducial camera, which can be used to identify the jetting of nozzles before and after printing, but not during the printing itself. The clogging of the nozzles appears on the samples in form of missing lines or areas. The example of such scanned catalytic layer (Anode 2) printed on PTFE substrate is shown in Figure 7. Furthermore, the non-printed areas can be filled in a second printing pass. Deposition of the ink will happen only at locations where it is required. Additionally, by varying contrast and brightness of the layer, it is possible to identify inhomogeneity of the printed layers from scanned images (Figure 7B).
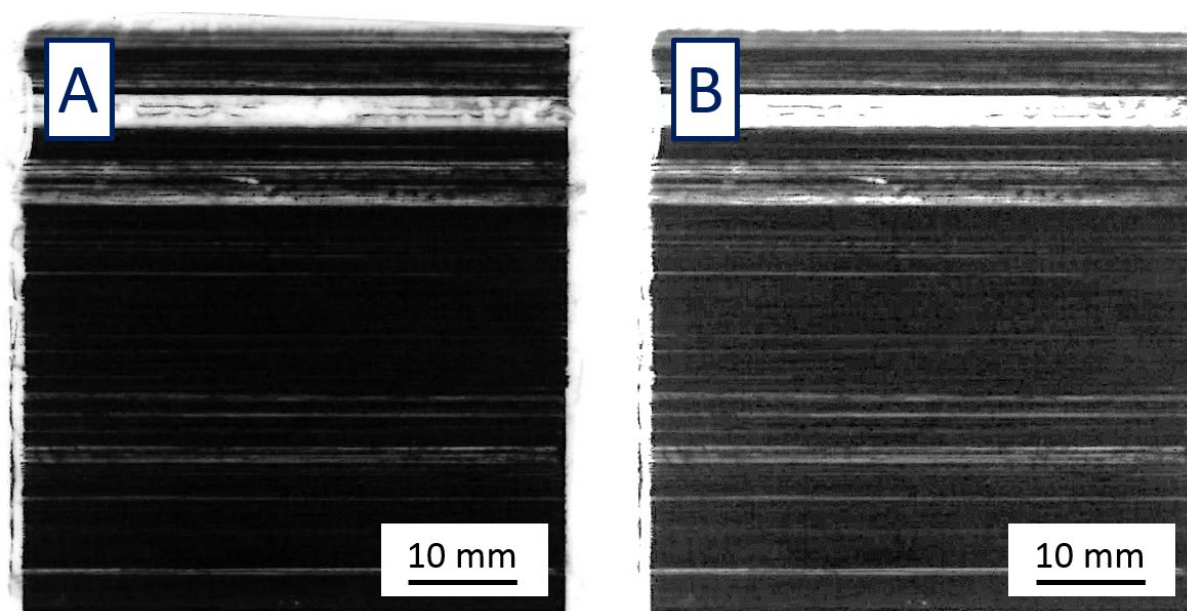
Figure 7 (A) Scanned inkjet-printed catalytic ink (Anode 2) on PTFE substrate; missing lines due to clogged nozzles (resolution 600 dpi); (B) the same image with adjusted contrast and brightness; inhomogeneity of catalytic layer becomes visible.

2.2.1.3. ASSESSMENT

The flatbed scanner can scan non-transparent objects. Particularly, it can be used for scanning catalytic layers printed on different substrates. Since the catalytic inks are black, they are easily identified on the surfaces of the white PTFE or transparent membrane. In contrast, almost transparent layers of ionomer and some seals are hard to identify with reflective light, therefore scanning is not suitable for the characterisation of those layers.

Assessing the quality of the deposited layers by a scanner is comparable to visual inspection using line cameras during quality control and can indicate the success rate when detecting defects (missing lines due to clogged nozzles) during mass production.

The extruded Teflon used as a reinforcement is not transparent, but becomes transparent when properly impregnated with ionomer. Using a suitable background, one can monitor the progress of the deposition process and quantify the uniformity of the resulting membrane based on its transparency.

Figure 8 Usability of Flatbed Scanner for CCM development

2.2.2. OPTICAL MICROSCOPY

Figure 9 Optical microscope, Hirox KH-8700 (source: JMFC)

Optical microscopy provides the fastest data, requiring minimal preparation of the samples for analysis. The work in MAMA-MEA used the Hirox KH-8700 shown in Figure 9, which is capable of magnifications of ×35 to ×2500.

The primary function of the microscope is to look at the surface of a sample. However, it is not wholly limited to surface defects. Using different filters and internal software, the microscope can provide additional data about surface roughness, composition and integrity.

In MAMA-MEA, a basic use of the optical microscope was effectively finding points of interest by scanning across the sample at low magnifications before increasing zoom for interesting features.

Whilst scanning over a sample, changing from a ring light to a coaxial light could show features that the other failed to highlight.

Coaxial light   Ring light
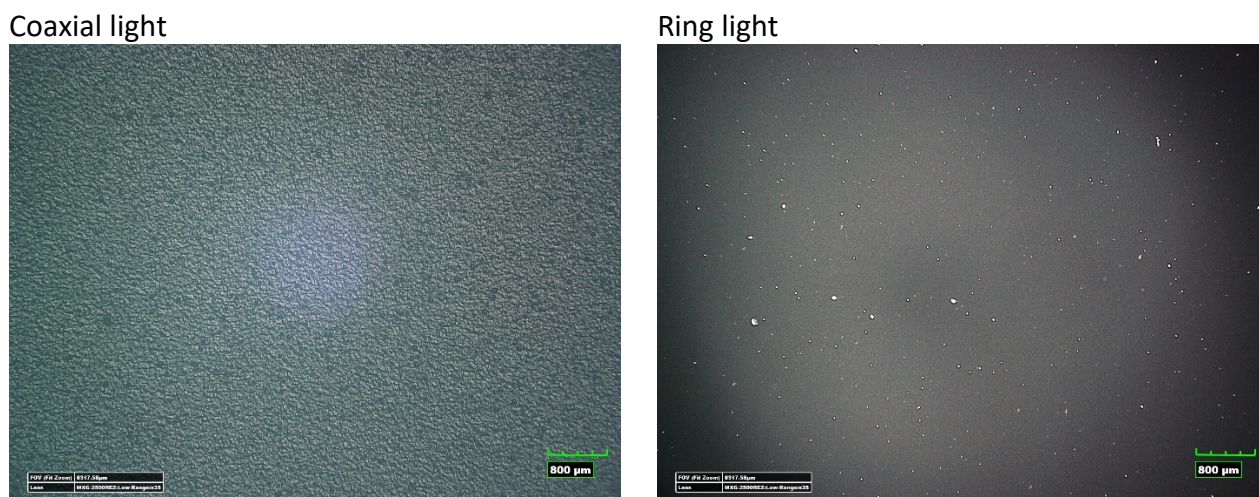
Figure 10 – A comparison of the different lights on the same membrane sample.

As seen in Figure 10, the MAMA-MEA membrane sample under coaxial light (left) was a highly textured light blue colour. The texture was due to undulations within the sample. With the ring light (right), there was less texture to the surface and the image was a natural black colour. Additionally, small white spots were visible, which indicated points of interest in the sample.

Opaque samples such as catalyst layers can be illuminated using a backlight. Any areas where catalyst is missing will allow the backlight to shine through the gaps, as shown in in Figure 11. Using this technique allowed characterisation of the missing print to be conducted to assess features such as crack size, cracked area, etc. Areas of interest can be identified by the scanner, analogically to what has been discussed in paragraph 2.2.1.3.

0.1 % cracking   1.4 % cracking
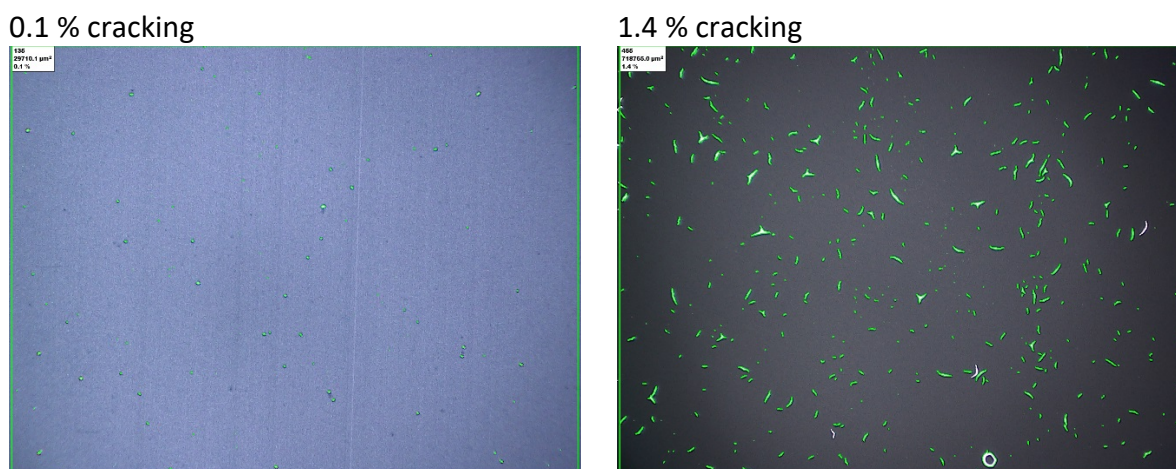
Figure 11 – Two different catalyst layers displaying different degrees of cracking

For each image in Figure 11, areas above a chosen brightness threshold were selected, giving a percent value of the total bright area over the total area within the photo. This method was also be used to give a qualitative measurement of areas where the catalyst layer is significantly thinned by adjusting the brightness threshold used to analyse the sample.

When qualifying the roughness of a surface, a 3D picture can be taken or constructed using e.g. focus variations. The picture is created via an inbuilt program which changes the camera height via small step changes, taking pictures at each step height. From each photo, any pixels in-focus are saved with an XYZ value. The program then builds an image from all the in-focus pixels.
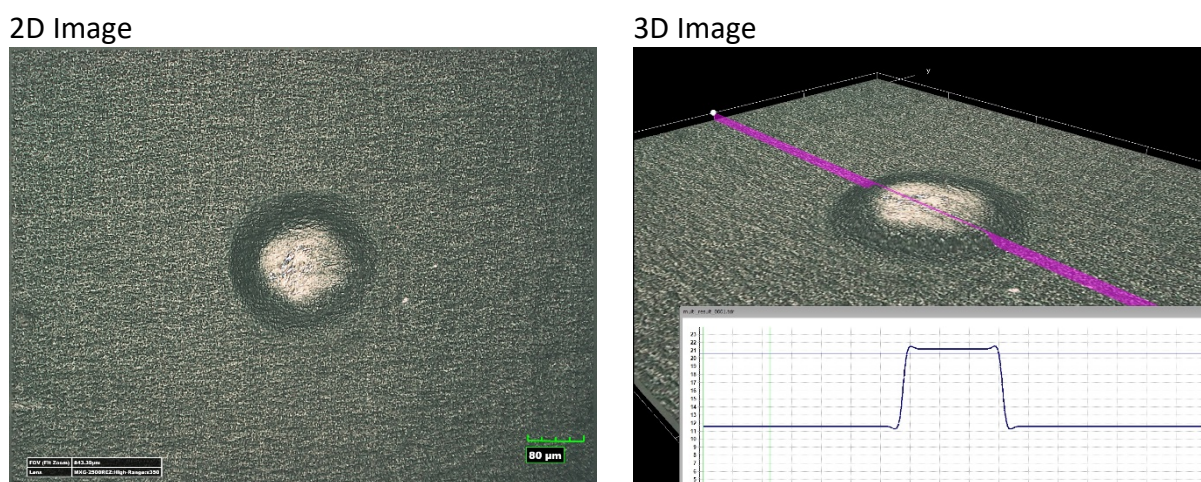
2D Image   3D Image

Figure 12 – A lump found within a membrane.

Figure 12 shows how a 3D image helped in clarifying what was unclear within the 2D image, as the 2D defect (left) could have been a lump or a dimple. With the 3D image (right) it became clear that the defect was a lump. It also provided a rough approximation of the size of the defect as profiles of the 3D space could be taken.

Figure 13 Usability of Optical Microscope for CCM development

2.2.3. SCANNING ELECTRON MICROSCOPE (SEM)

The SEM is used to complement analysis from the optical microscope. Non-conductive samples such as membranes needed to be coated in a fine gold layer to stop charging, whilst conductive samples needed no preparation. The SEM used for the MAMA-MEA work was the JEOL JCM-5000, as shown in Figure 14, with ×10 -- 20,000 magnification which detects both back-scatter and secondary electrons indiscriminately.

Figure 14 – JEOL Neoscope JCM 5000, Scanning Electron Microscope (source: JMFC)

With the SEM providing a greater resolution than the optical microscope, it is effective at taking higher magnification pictures without loss of resolution.

Optical microscope   SEM
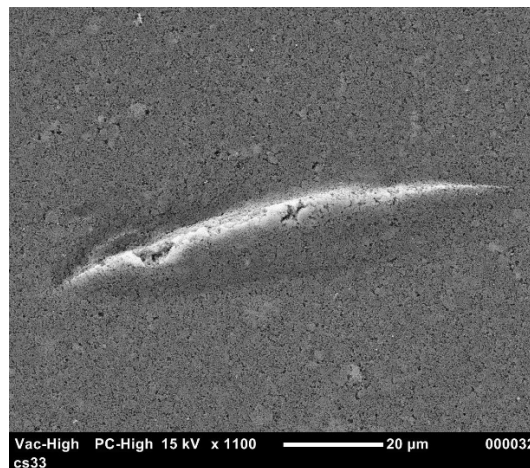
Figure 15 – Catalyst defect investigated using optical microscope and SEM

The feature shown in Figure 15 lacked detail when looked under the optical microscope (left). Under SEM (right), the texture of the catalyst was clearly visible, with the ridge-like structure showing missing pieces of catalyst along its apex.

Optical microscope
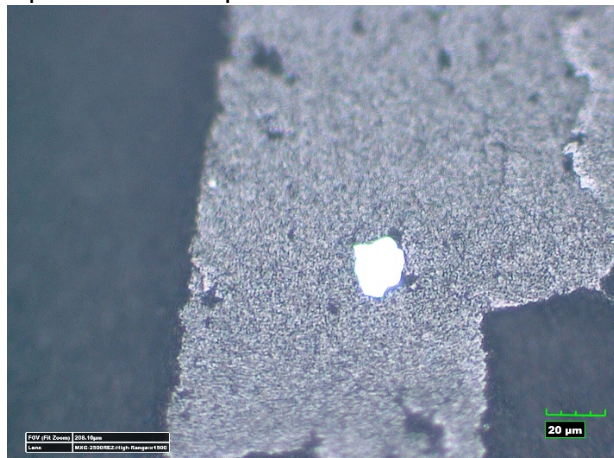
SEM
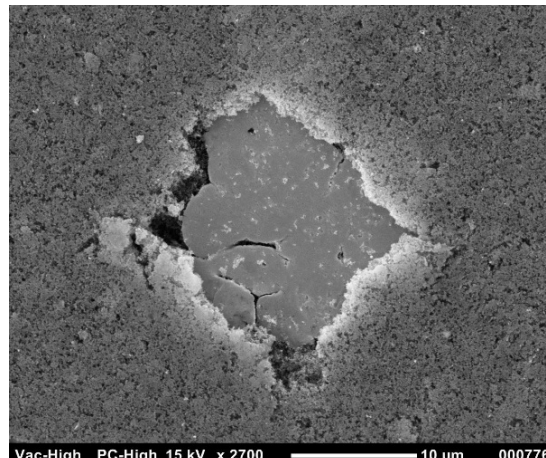
Figure 16 – Catalyst defect investigated using optical microscope and SEM

In Figure 16, the SEM (right) provided more detail than the optical microscope could provide (left). Using the optical microscope, the feature was very bright, making it difficult to ascertain the detail and exactly what it was. Under SEM the feature was more clearly visible and could be seen to be missing catalyst.

Figure 17 Usability of SEM for CCM development

2.2.4. CROSS-SECTIONING

Cross-sectioning was used to look in more detail at the composition of samples with focus on the relative thicknesses of layers as well as their interaction with each other. Cross-sectioning requires a

Figure 18 – Buehler AutoMet Grinder-Polisher (source: JMFC)

longer preparation procedure than top down microscopy, but this is necessary as care must be taken to ensure that all of the sample is polished to the same focal length, and that no damage is done to the sample during preparation.

Representative samples were cut from the material of interest and set in epoxy resin. Once set, the sample was then polished to give a flat surface using a Buehler AutoMet Grinder-Polisher (Figure 18). The polishing was done over several stages, with each progressively finer than the previous.
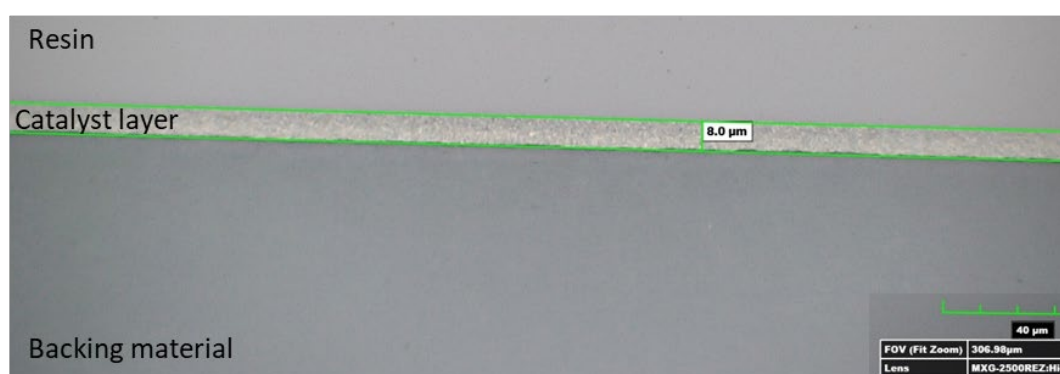
Figure 19 – Catalyst cross-section under optical microscope

Figure 19 shows a cross-section of a catalyst layer attached to a backing layer. This provided insight into the consistency and thickness of the catalyst layer. This can be helpful when looking at Pt loadings, as the cross-section can tell you whether the Pt loading is low due to lack of catalyst (thin layer) or inhomogeneous.

Cross-sections were also be viewed under the SEM (Figure 20). Due to the non-conductive surface of the resin, samples needed to be coated in a fine layer of gold or carbon and grounded using carbon tape.
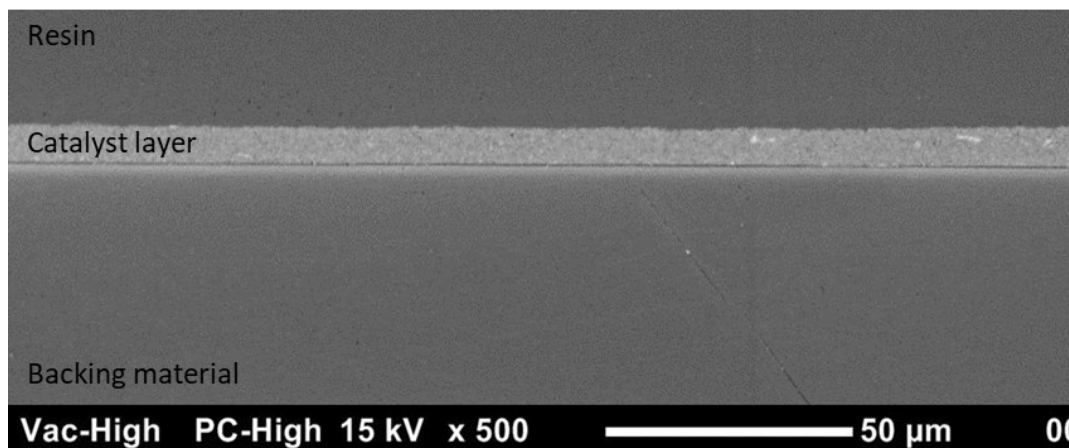
Figure 20 – Catalyst cross-section under SEM

Cross-sectioning could also be used as an effective way of characterising points of interest in the layers.

X35 magnification   X350 magnification

Figure 21 – Defect found upon a CCM

Figure 21 shows a small defect that was present inside a much larger one. 35 times magnification (left) showed a circular defect with a small defect within. 350 times magnification (right) gave a close-up of the smaller defect. From the microscopy alone it was hard to determine the composition of the defect.

To cross-section a defect like this, a marking technique was used.

Marked top down
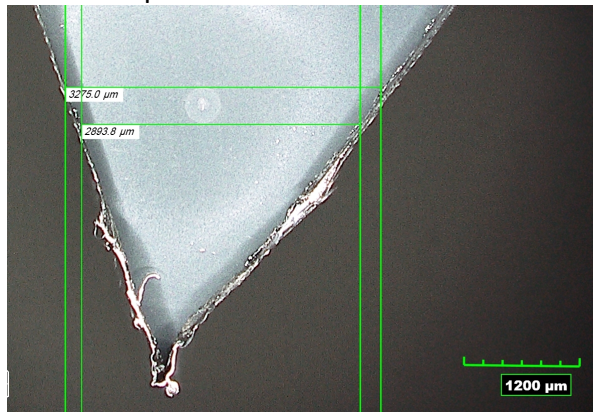
Cross-section
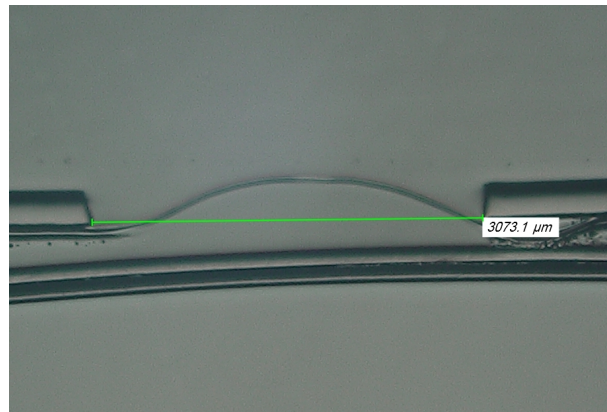
Figure 22 – Left shows the top down marked defect. Right shows the cross-section of the defect.

Figure 22 (left) shows the marker, which was tape with a V cut out. This was then stuck to the CCM with the defect inside the V. A width measurement between the carbon tape edges was taken from the top and bottom of the defect as shown. This showed that the location of the defect was between ~3300 and ~2900 μm carbon tape width. The sample was then prepared in cross-section as discussed previously. The sample was polished until the desired width was found as seen in the cross-sectional image of Figure 22 (right). This indicated that the defect should be within this cross section, which could then be analysed.

2.3. TACTILE PROFILOMETER

2.3.1 DESCRIPTION

Figure 23 and Figure 24 show the profilometer Dektak 150 from Veeco, available at Fraunhofer ENAS. The device is placed on a vibration-damped table.
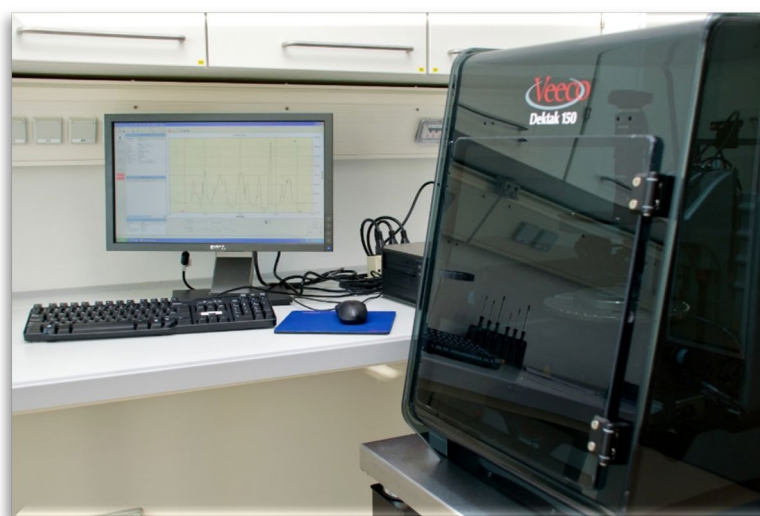
Figure 23 Work place of the tactile profilometer (source: ENAS)

Furthermore, the encasing of the device is necessary to avoid influence on the measurement results by air fluctuations. A usual application field is the measurement of wafer structures. In this project, the device is used to measure various deposited layers on polymer substrates.

The working principle is that a cantilever with a tiny needle tip is directed onto the surface of a sample. When contacting the surface, the force is recognised and used to measure the distance in z-direction. Then the stage is moved in x/y-direction to scan the surface in straight lines. Proceeding this scan movement, the z-height is controlled and recorded. Based on these data the **roughness** can be recorded according to the preferred method.

To measure a **layer thickness,** the heights of the carrier substrate as well as of the layer on top are determined. This turns out to be sometimes very challenging. Taking some film carrier or even membrane material as substrate, the surface is very wavy and mostly not planar. The software offers an option to level the measurement lines to get rid of this effect to some degree. To determine the layer thickness, it is mandatory to have both levels (substrate and layer) with high accuracy. To ensure most reliable measurements, the scans should start at the substrate level, cross the deposited layer, and end at the substrate level. Therefore, the most accurate levelling can be realized.

Figure 24 Close up of the cantilever probing a sample (source: ENAS)

The measurement of the **morphology** in line scans is relatively easy. To determine the morphology of an area the approach is to perform a number of parallel line scans and to combine these data. Depending on the size of the area, this measurement procedure can require from several minutes up to hours.

Table 1 Dektak 150 Specification (Selection from (2))

Parameter	Value
Scan Length Range	55 mm
Data Points Per Scan	60,000 max.
Max. Sample Thickness	Up to 100 mm
Max. Wafer Size	150 mm
Step Height Repeatability	6 Å
Vertical Range	524 µm standard; 1 mm optional
Vertical Resolution	1 Å
Stylus Force	1 to 15 mg with LIS 3 sensor
Stylus Options	Stylus radius options from 50 nm to 25 µm

In Table 1, selected parameters from the data sheet of the device are given. The overall sample size is limited to a circular disc size with a diameter of up to 150 mm. The stage consists of a porous material, so that a vacuum can be used via the mounting stage to fix the sample. When measuring wafers, this setup ensures an even basis for all measurements. Nevertheless, when processing wafers there might be a tilt angle > 0° which can be compensated by software alignment. Changing the sample into a polymeric film material, this even basis for measurements is no longer available. Polymeric films show a reduced planar surface with deviations across the surface that might be in the range of tenths of micrometres. Therefore, the measurement of any sample requires a good calibration and compensation.

The big benefit of a tactile profilometer is that independently of any layer colour (e.g. black, transparent) the measurement approach is performing well. Optical recognition of surfaces often requires dimensions in the order of the wavelength of the sensing light (i.e. 400 - 800 nm). Sometimes the layers are much thinner and therefore cannot be determined in this way. For layers under investigation in MAMA-MEA this limitation is not evident because the intended layer thickness is in the range of several micrometres.

There can be three challenges that might apply with this technology: Firstly, the measurement process is sequential, i.e. each point is determined individually, resulting in higher demand of measurement time. Secondly, in very soft layers the tip could cause such pressure that it dips into the surface, resulting in incorrect measurement values. Thirdly, using the vacuum chuck may cause a nonuniformity of water content in the membrane over longer time periods influencing the measured values.

2.3.2. Measurement results

The result of a tactile profilometer line measurement is given as a xy-graph. The abscissa (x-axis) displays the scan length, usually in µm or mm scale. The ordinate (y-axis) displays the height, usually in µm scale. In Figure 25, a line scan of an anode layer printed by inkjet-printing onto a membrane substrate as well as the estimated substrate level (green line) is shown. Within 4.5 mm of measurement range, there is a deviation of 3.7 µm of the substrate level. In this sample a severe nozzle clogging can be detected. Nevertheless, this sample explains the usability of a tactile profilometer well. The substrate layer determines the measurement result significantly. The layer thickness varies between 0 µm and about 7 µm. The following height information while scanning towards 4.5 mm fluctuates nearly regularly. This is a clear influence of the substrate underneath of the catalyst layer.
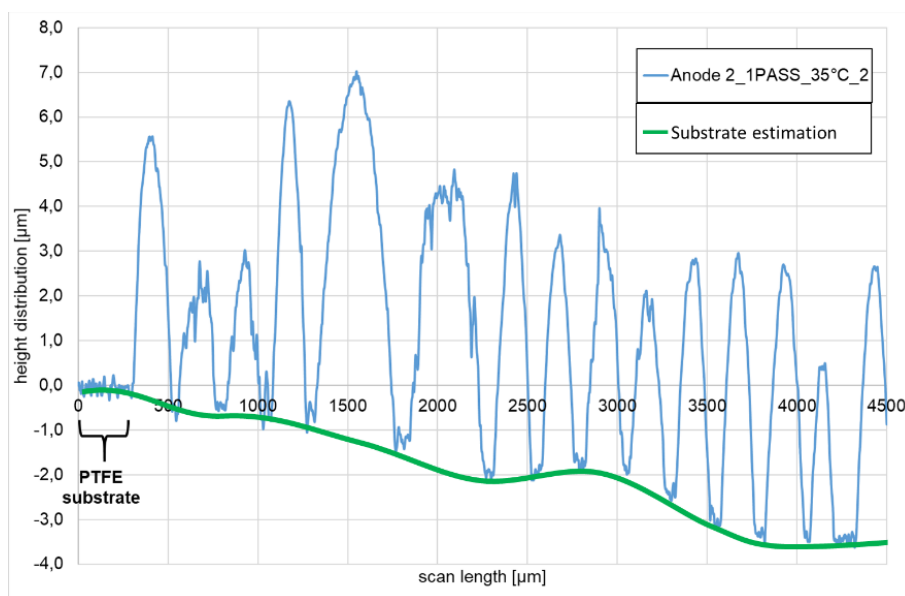
Figure 25 Scanned surface line of an inkjet-printed anode layer with nozzle clogging and additional substrate estimation (green line)
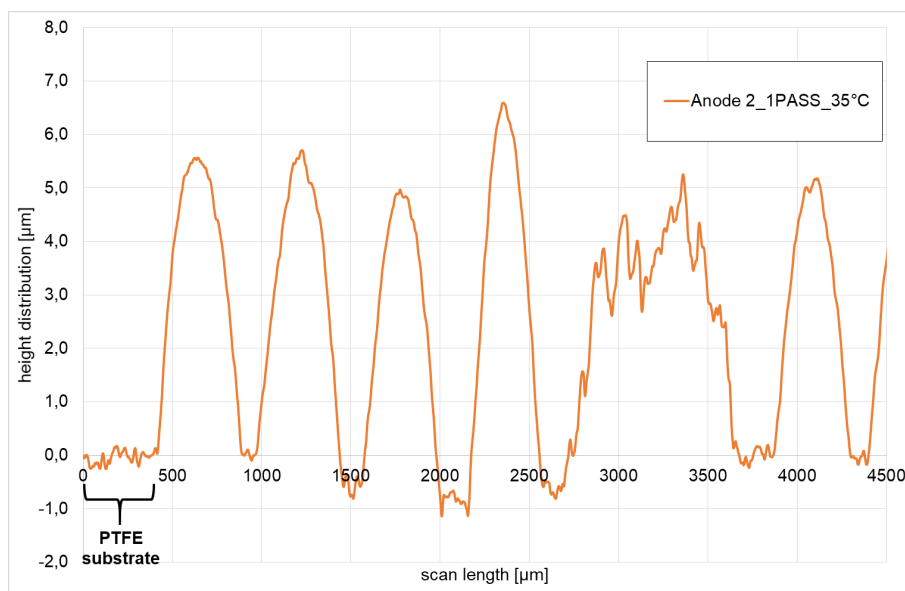
Figure 26 Normalized layer thickness (different sample than Figure 25)

In Figure 26, the normalized scan line (i.e. the calculated measurement result, after subtracting the level of the substrate) across an inkjet-printed anode layer is shown. In this graph, there is a very clear separation between single lines of about 570 µm. Just two lines are merged (between 2800 µm and 3600 µm). These two lines generate a joining with severe roughness. The other lines are much smoother.

What can be concluded is, that a flexible substrate like a membrane is challenging for determination of layer thicknesses.

2.3.3. ASSESSMENT

Tactile profilometry is a very versatile lab measurement method originally intended for stiff substrates like silicon wafers or glass. This device has the clear advantage that a direct contact between tip and sample delivers information despite any optical restriction like black or transparency.

The employment for CCM manufacturing is useful – although there are some restrictions. The main challenge is to measure layer properties on non-planar substrates. The beneath substrate like PTFE film or membrane is typically very rough. This roughness cannot be levelled in every case, so that measurement results need an experienced interpretation. The best measurement results can be achieved where material is deposited only in small stripes. In this case a levelling can be done quite easily. In contrast the determination of large layers thickness distribution may become very challenging because no reliable reference to the substrate is given. Due to the inherent speed, tactile profilometry is not suitable for inline quality control.

Figure 27 Usability of the tactile profilometry for CCM development

2.4. FUNCTIONAL LAYER CHARACTERISATION

2.4.1. ELECTRICAL PROBE STATION

2.4.1.1. DESCRIPTION

The workplace of the electrical probe station is shown in Figure 28, while Figure 29 shows a close-up of the four contact needles on a sample. The original market for this equipment is for electrical contact of devices manufactured on a wafer. For a better positioning, a binocular microscope as well as illumination is placed above the measurement table. The table itself can be manually directed in x-y-z-direction. The probe needle foots are fixed by a magnet onto the mounting table. Adjustment screws allow a very precise/fine movement of the tips.
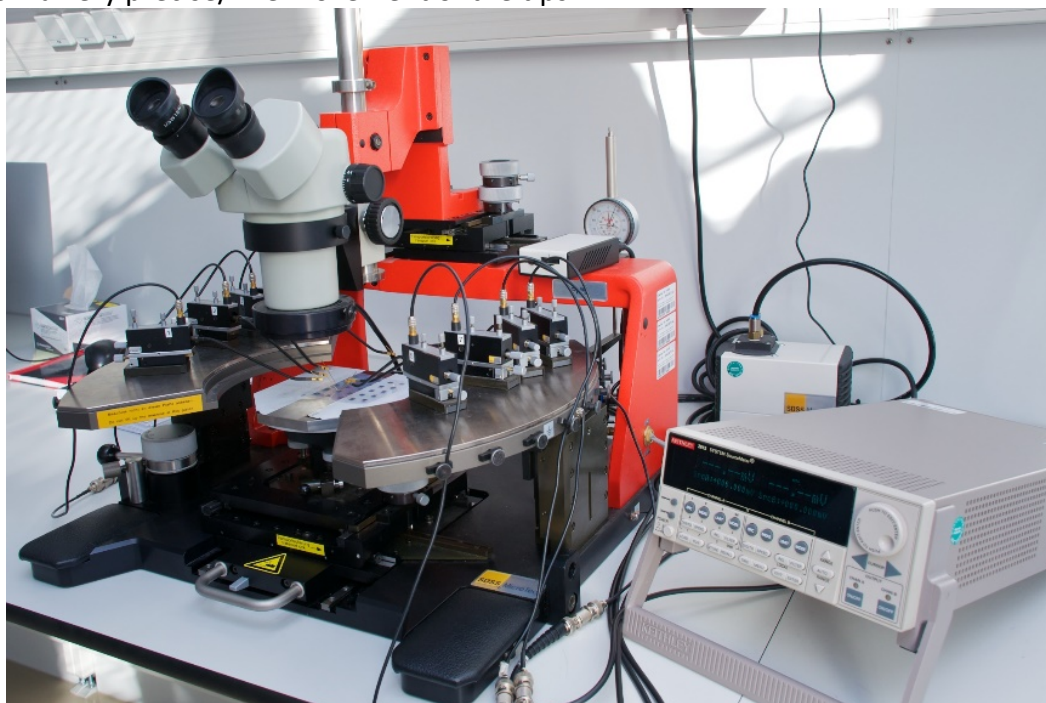
Figure 28 Suess MicroTec probe station PM5 with Keithley 2612 SourceMeter (source: ENAS)

The electrical probe station itself only enables a defined placement and interface of an electric tip in respect to a sample. In the MAMA-MEA project, the samples are printed or coated layers on a polymeric carrier. The carrier is fixed to the table either by vacuum or by adhesive tape. The other

end of these electric wires can be connected to the measurement equipment used (here Keithley 2612 SourceMeter).

In the easiest application, the ohmic resistance of a line of a defined length is measured by a pair of tips and a multimeter. The multimeter generates a voltage and determines the flow of current. Based on Ohm's law the resistance can be determined. Taking the distance of both tips into calculation, the unit of this measurement result is $[\Omega/m]$. To overcome inaccuracies in conductive line measurements, one may separate the introduction of a current flow and the measurement of the resulting voltage. This is called four-terminal or Kelvin probe. This measurement is done in-plane and delivers accurate results only for line conductors. Measurement of conductive areas can just give an indication.
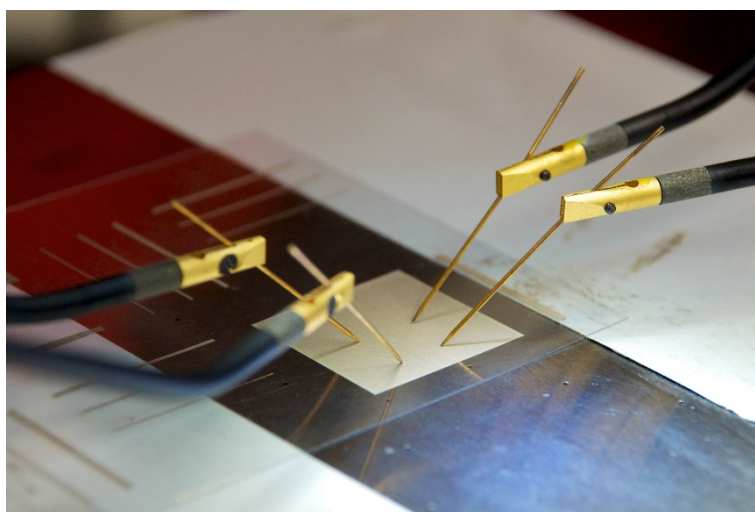
Figure 29 Needle setup for van der Pauw method surface resistance measurement (source: ENAS)

To overcome geometrical dependencies, usually four tips are employed to measure the surface resistance according to the van der Pauw method, as shown in Figure 30.

1. Measurement

$$R_{12} = \frac{U_{34}}{I_{12}}$$
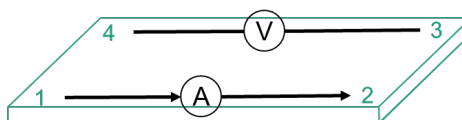
2. Measurement

$$R_{23} = \frac{U_{14}}{I_{23}}$$

Homogenous sample: $\frac{R_{12}}{R_{23}} = 1$

Figure 30 Van der Pauw measurement setup. To introduce current I, a source A is used; to measure voltage U, a voltmeter V is used.

In the basic approach, one pair of contacts introduces a current I while the second pair of high-ohmic contacts measures the voltage U. The current for measurements are tuned between 10 µA and 1 A, so that the resulting voltage can be measured by the Keithley instrument.

Due to the resistivity of the layer a voltage drop across the current path arises, which is measured via the second pair of contacts. This measurement is performed a second time while rotating the measurement direction by 90 °. If the distance of contacts is equal and the sample is homogenous the ratio of both measurements will become 1. If there is any deviation from a square (w.r.t. the placement of the four tips) or the sample is inhomogeneous, the ratio will be either less or greater than 1. In this way, also effects of the printing direction can be identified. The unit of this measurement result is [$\Omega/\square$].

By taking the layer thickness into account the specific resistivity [Ωm] can be determined.

2.4.1.2. MEASUREMENT RESULTS

When just measuring a line resistance, the distance of the two tips needs to be taken into account to calculate the specific conductivity. A sample result is given in Figure 31. When performing this measurement for a large set of samples, the deviation in conductivity values can indicate a deviation in layer thickness or even in layer quality.
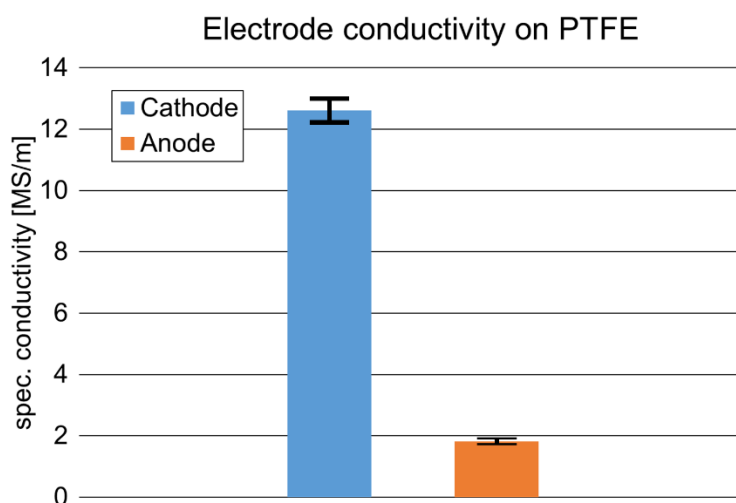
Figure 31 Conductivity of Anode and Cathode electrodes slot-die coated on PTFE (error bars indicating standard deviation of five measurements)

By employing the van der Pauw measurement setup, the conductivity is measured not along a line, but across the included area. A sample measurement result is given in Figure 32.
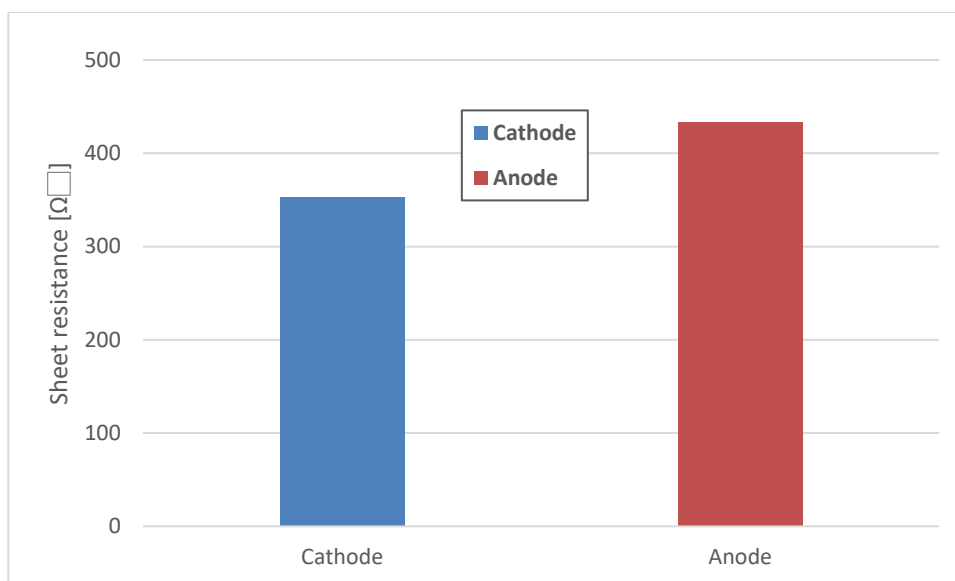
Figure 32 Sheet resistance (van der Pauw setup) of Anode and Cathode electrode slot-die coated on PTFE

The results shown in Figure 31 and Figure 32 are measured with different samples. Nevertheless, the tendency is demonstrated: a high specific conductivity belongs to a low sheet resistance, and vice versa.

2.4.1.3. ASSESSMENT

Measurements done in the electrical probe station can be a versatile way to quickly check the electrical properties of the deposited layers. Although small errors cannot be detected, a deviation in layer thickness or severe cracks might be identified. The challenge with this type of measurement is the requirement of a direct contact to the sample – that needs to be fully dried for this evaluation. The setup itself is robust.

Figure 33 Usability of probe station for CCM development

2.4.2. ELECTROCHEMICAL TESTING

The 25 cm^2 CCMs produced by multi-layer additive layer manufacturing (ALM), i.e. deposition, were characterised. Electrochemical active surface area, hydrogen crossover current, cell resistance and cell performance were measured to assess the functionality of the resulted CCMs, including their comparison to benchmark CCMs to assess performance parity.

The evaluation of the electrochemical active surface area (ECSA) based on cyclic voltammetry, quantifies the accessible and active sites, i.e., the available surface area of catalyst particles, which determine the reaction kinetics and thus the electrochemical performance. The comparison of the results to the benchmark allows the assessment of how the ALM fares with respect to conventional deposition methods. The performance of the ionomer in the CCM is examined via hydrogen crossover and temperature sweep. The gas crossover quantifies the permeation of hydrogen in a molecular form through the membrane and corresponds to the ability of the membrane to separate the anode and cathode compartments, as well as determines in part the highest attainable cell voltage. The measured value of transport limiting current is obtained by linear sweep voltammetry with humidified hydrogen at the anode and nitrogen at the cathode. The temperature sweep test from benchmark testing protocol can give a reference on how membrane would react to humidification cycling, as well as potentially demonstrate the mechanical stress on membrane during the testing. As a proof of concept, polarization curves under various operating conditions were recorded to provide one of the main KPIs (power density of 0.67 W cm^2). In addition, electrochemical impedance spectroscopy was employed at the end of the protocol to obtain the cell resistance relative to that of the reference CCMs. All tests were conducted using FuelCon test bench with test cell fixture quickCONNECT qCf FC25 by BalticFuelCells GmbH and Solartron Modulab potentiostat booster 12 V/20 A by AMETEK, Inc, see Figure 34. The vertical orientation of test cell, shown in Figure 35, was adopted for some of the tests to alleviate issues stemming from the anode flooding experienced initially with the original flow field. An alternative flow field has been procured to rectify the issues and get higher quality data for the comparison with the benchmark.
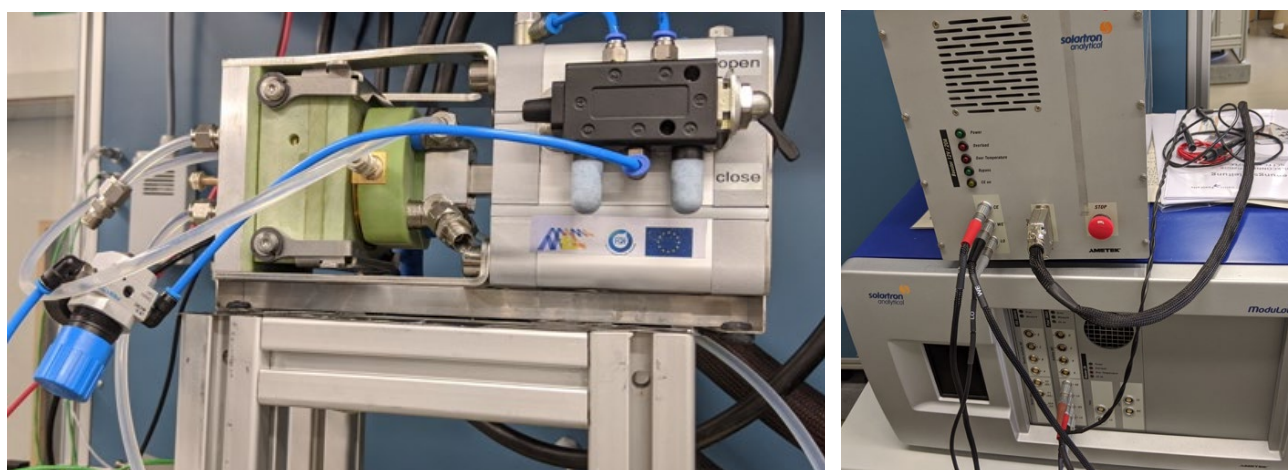
Figure 34 Electrochemical testing equipment: balticFuelCells test cell fixture on the left, Solartron potentiostat module with a 20 A booster on the right. (source: TUC)
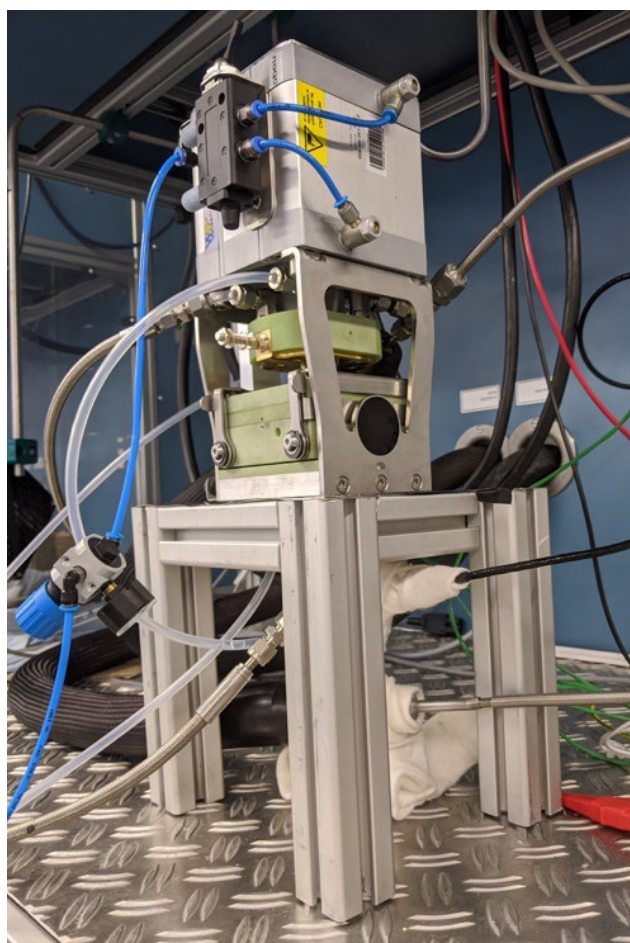
Figure 35 Vertical positioning of test cell fixture, anode at the bottom. (source: TUC)

2.4.2.1. CYCLIC VOLTAMMETRY: ELECTROCHEMICAL ACTIVE SURFACE AREA

Cyclic voltammetry is typically based on CO or hydrogen sorption. Hydrogen sorption was used, because CO could cause suffocation in mass manufacturing environment. The cyclic voltammetry was carried out with ALM MEAs and conventionally-made reference MEAs to compare the performance of the CCMs produced by ALM to the commercially available benchmark. The values of ECSA were calculated from cathodic adsorption area representing hydrogen adsorption sites on cathodic catalyst. Typical measurement results are shown in Table 2 and Figure 36. In Figure 36, a long tail below 0.1 V represents the evolution peak of hydrogen molecules; hence, in the calculation, it is subtracted from the integral area of hydrogen adsorption.
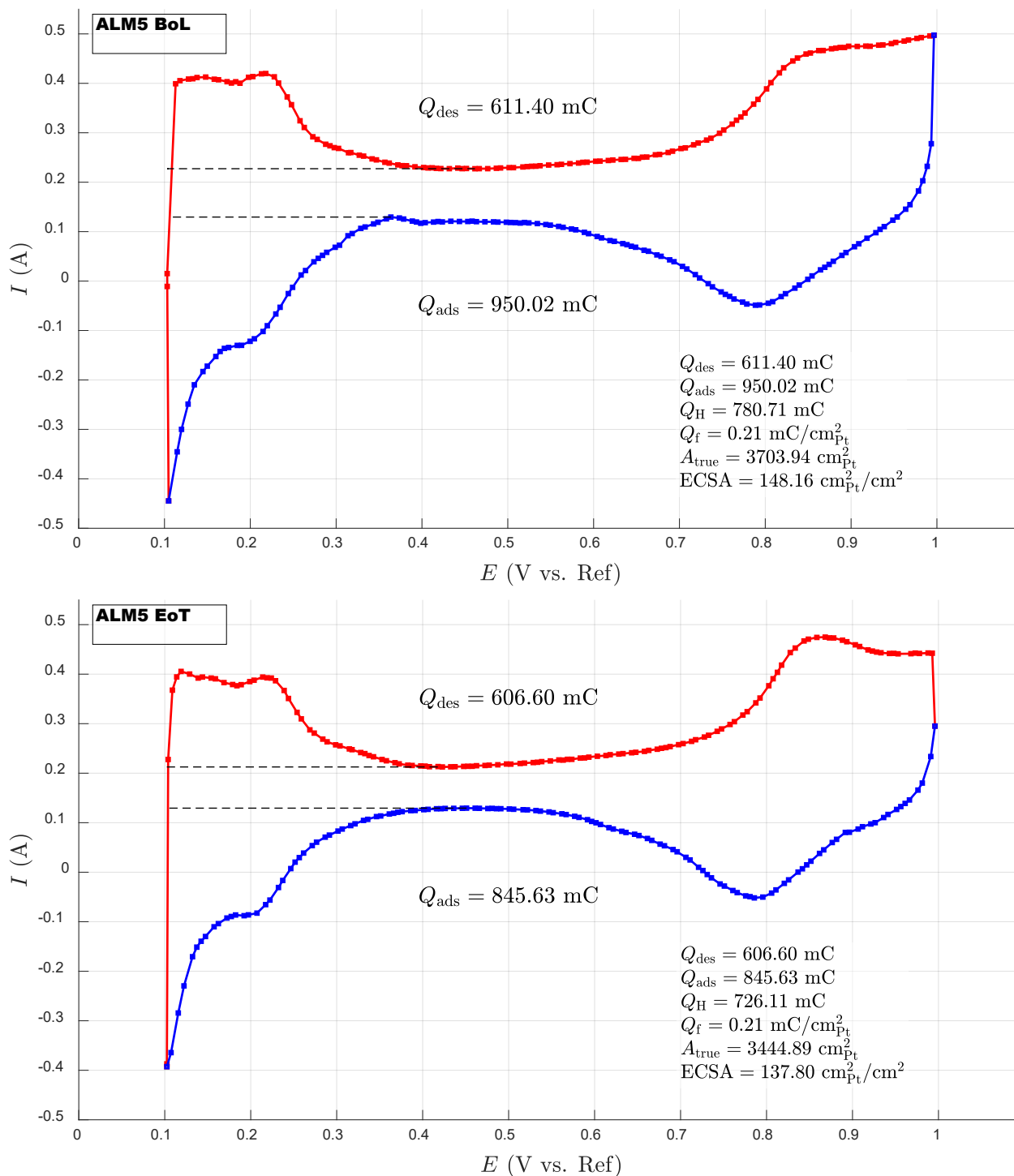
Figure 36 Example results of cyclic voltammetry from 0.1 V to 1 V vs RHE using scan rate of 50 mV/s at BoL (top) and EoT (bottom) for sample 5 of ALM MEA using a modified flow field with an active area of 25 cm^2.

The areas evaluated in both cases presented in Figure 36 considered the double layer region from around 0.4 V to 0.6 V as the baseline (between black horizontal lines) identified the search for local extremes. Scanning starting from 0.1 V reduced the effect of overlap from hydrogen evolution.

The results are only qualitative and serve for the comparison of the ALM MEA against the reference.

Table 2 Example Measurements of Electrochemical active surface area of the cathode

Sample	State	ECSA (cm^2-Pt/cm^2)
BENCHMARK*	BoL	191.0
REFERENCE MEA	BoL	150.72 ± 6.95
REFERENCE MEA	EoT	140.39 ± 9.06
ALM MEA	BoL	139.60 ± 14.19
ALM MEA	EoT	118.88 ± 7.20

*   Commercial MEA measured with CO stripping

ASSESSMENT

Although CO stripping is usually more accurate, because the cut off voltage does not lie in the measurement range (in our case, the cut off voltage of 0.1 V vs RHE impacts the integrals representing the charge stored in the sorption of hydrogen and in turn the ECSA measurement). ECSA is a crucial parameter reflecting the quality of the deposited catalyst layer because it captures the area of the catalyst available to electrochemical reactions.

According to ECSA values in Table 2, the active surface area of ALM MEAs resembles that of reference MEAs and benchmark. The values at EoT did not show significant decrease compared to that at BoL after the full set of tests of the reference protocol. Such trend could be attributed by the clearing of the solvent residua with the first test CV passes at BoL giving a lower apparent ECSA, skewing the comparison. ECSA values of ALM MEA are comparable to reference and benchmark, meaning the catalyst layer of ALM CCMs possess a sufficient electrochemical activity.

Cyclic voltammetry is applicable at lab-scale in research, but currently not suitable for mass production, as visualised in Figure 37 by the full and empty marker. The marker is separated in the following sections to compare the usability in the lab and fab environment for techniques that can be implemented in both contexts. CV does not detect microscopic details (microelectrodes, analogical to tactile measurements described in paragraph Tactile Profilometer, allow microscopic characterisation but are time consuming and only pertain to a small area), but can aid ink development and deposition technique selection. As for the usability of CV, the method is well established at the lab scale, but the implementation in mass manufacturing lines with the web speeds in metres per second would be a challenging endeavour.

Figure 37 Usability of cyclic voltammetry for catalyst layer characterisation. Filled marker indicates the lab-scale and the empty marker the fab-scale usability, respectively.

2.4.2.2. LINEAR SWEEP VOLTAMMETRY: HYDROGEN CROSSOVER

To quantify the value of hydrogen crossover, linear sweep voltammetry was applied to ALM and reference MEAs. Current density recorded along voltage variation is converted to hydrogen crossover flux. The limiting current density is calculated from measurement points past the initial transient, which is identified by the derivative of the current density approaching zero. Typical measurement results are shown in Figure 38 and Table 3, filled markers denote the points considered in the calculation.
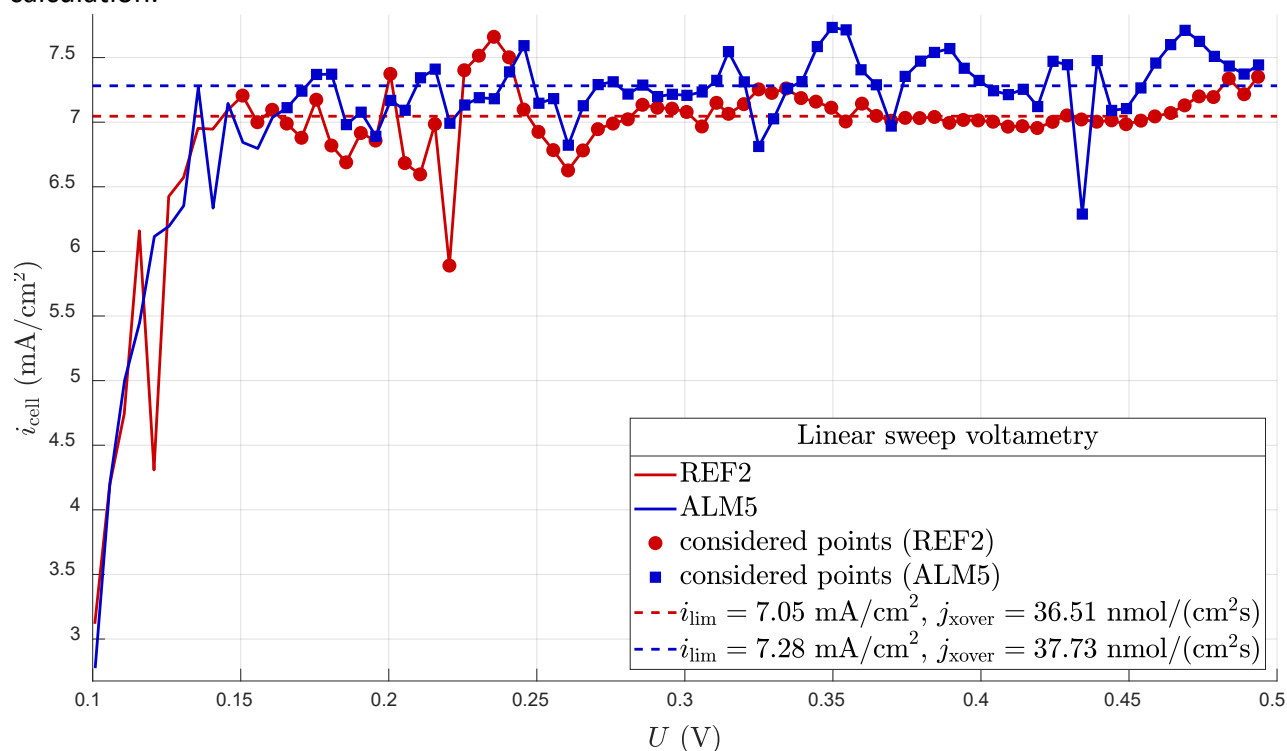
Figure 38 Comparison of Linear Sweep Voltammetry cropped to 0.1 V to 0.5 V of reference MEA (red & circle) and ALM MEA (blue & square) at EoT. The points used in computing the limiting current density were selected using points in which the absolute value of the first forward difference was under 1 standard deviation.

Figure 38 shows that current density stabilised in the range of 7.0 - 7.5 mA/cm^2 from 0.15 V onwards. The values in Table 3 were calculated from eight samples for each material and the low variation indicates that the permeability is consistent across several batches.

Table 3 Example measurements of Hydrogen Crossover

Hydrogen crossover -EoT	Transport limiting current density, i_{lim} (mA/cm^2)	Hydrogen crossover flux j_{xover} (nmol/(cm^2 s))
REFERENCE MEA	6.88 ± 0.18	35.66 ± 0.92
ALM MEA	7.54 ± 0.23	39.08 ± 1.20

ASSESSMENT

For evaluation on hydrogen crossover in Table 3, the values of ALM and reference CCMs did not show a notable difference, proving low gas permeability of ALM CCMs, which is a crucial property of a CCM in fuel cell applications. As with other lab-based methods, the implementation in a mass production environment would be challenging and the evaluation would perhaps need to rely on larger applied voltages and the limiting current density derived from the transient data.

Figure 39 Usability of linear sweep voltammetry for layer characterisation. Filled marker indicates the lab-scale and the empty marker the fab-scale usability, respectively.

2.4.2.3. TEMPERATURE SWEEP

The test temperature ranged from 50 °C to 90 °C in 10 °C increments with a constant humidity corresponding to dew point of 50 °C. Cell voltage at current density of 1.2 A/cm^2 was recorded for 1 h at each temperature, including the ramp-up and equilibrium. Since there is a protection mechanism in the test protocol to prevent undesirable damage to the tested cell, cell voltage below 0.2 V would interrupt the measurement. As can be seen in Figure 40, the actual highest temperature for all MEAs could not reach 90 °C. Therefore, 85 °C was selected as the substitute highest temperature. Example results are shown in Figure 40 and Table 4. The graphs show the transition of the cell voltage after a change in the cell temperature resolved in temperature and time domain. Above 70 °C, temperature increase results in the reduction in the cell voltage that can be attributed to the decreasing relative humidity and, hence, the conductivity of the ionomer in the CCM. ALM CCM was comparable to the reference MEA, but neither of the samples reached the cell voltages recorded for the benchmark.

Table 4 Cell voltages for temperature sweep test

V @ 1.2 A/cm^2 at 50 DP	50 ℃	60 ℃	70 ℃	80 ℃	85 ℃
BENCHMARK*	0.59	0.60	0.59	0.52	0.45
REFERENCE MEA	0.51	0.51	0.50	0.41	0.34
ALM MEA	0.50	0.44	0.47	0.41	0.23

*   Reference data provided by JMFC
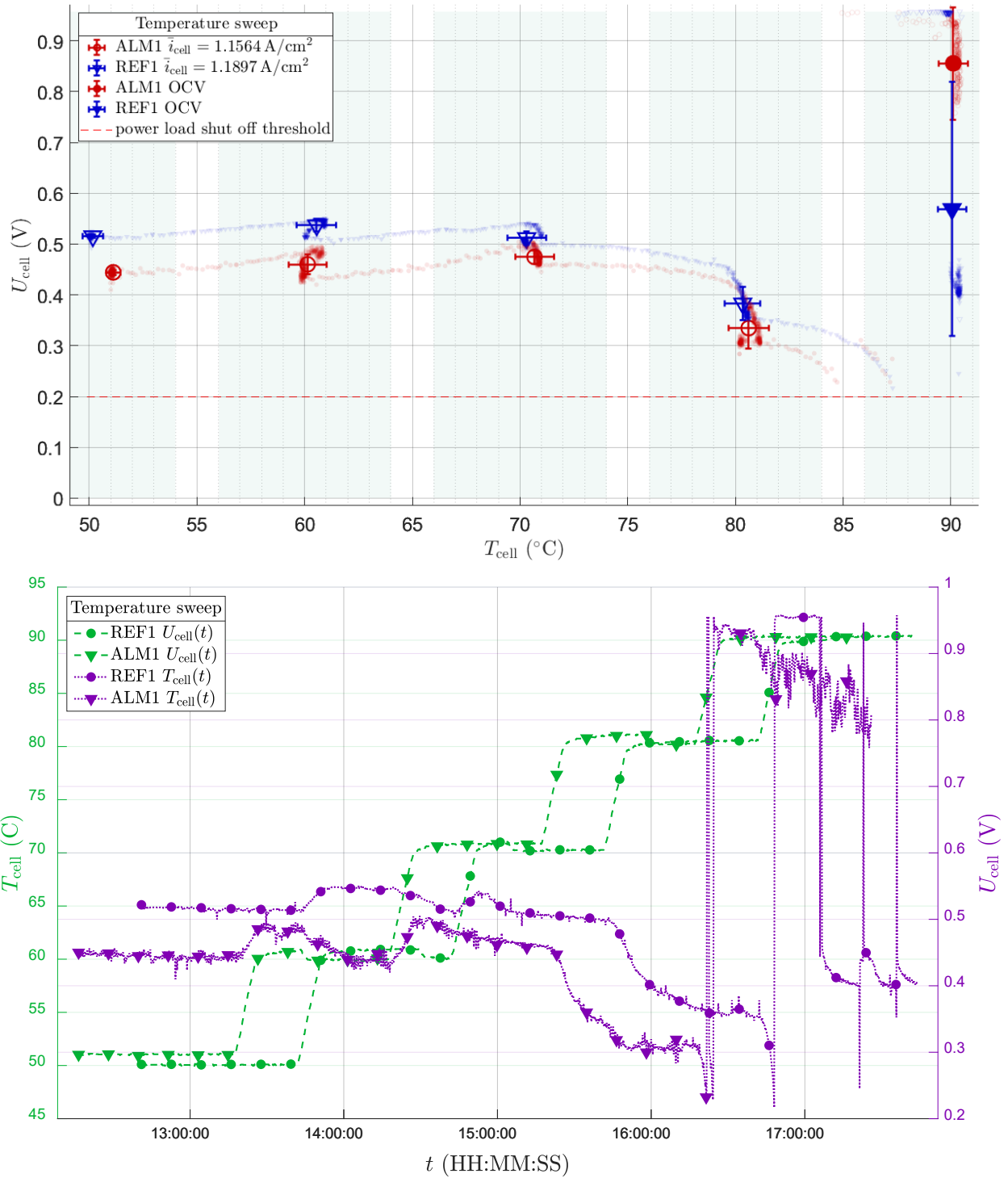
Figure 40 Cell voltage at 1.2 A/cm² of reference MEA and ALM MEA, with temperatures from 50 °C to 90 °C with humidification maintained at 50 °C dew point. Along with the voltage in temperature domain (top), the evolution of voltage and temperature in time domain (bottom) is provided for context. The power load was set to interrupt the measurement for cell voltages under 0.2 V, resulting in the OCV tails at temperatures above 85 °C.

ASSESSMENT

The recorded voltages in temperature sweep for ALM are lower than those of reference MEAs in Table 4 and both are lower than a commercially available benchmark used within the project. Issues with anode flooding (alleviated with the vertical orientation and the use of an alternative flow field) demonstrate that flow configuration may noticeably impact the outcome of this evaluation method. On the other hand, the ability of water retention in membrane was observed from the results to maintain the consistent performance at moderate current density under desired conditions. Although temperature sweep is useful in the lab environment to probe the impact of temperature and humidity on the CCM performance, it would be difficult to implement this technique in a mass manufacturing environment.

Figure 41 Usability of temperature sweep for layer characterisation. Filled marker indicates the lab-scale and the empty marker the fab-scale usability, respectively.

2.4.2.4. CELL RESISTANCE

To understand and verify the functionality of membrane, cell resistance is a sole diagnostic parameter that stands for ohmic resistance of CCMs relative to membrane resistance. The values of cell resistance were determined by the intercept at X-axis of the semicircle within the range of high frequency in Nyquist plot in Figure 42 from electrochemical impedance spectroscopy and the active area of CCMs. As a side note to the noise within the part of low frequency can be attributed to instrumental artifacts or flooding effect of the cell, which could be neglected due to less significant impact on high frequency. The results are shown in Table 5 compared to an internal benchmark.
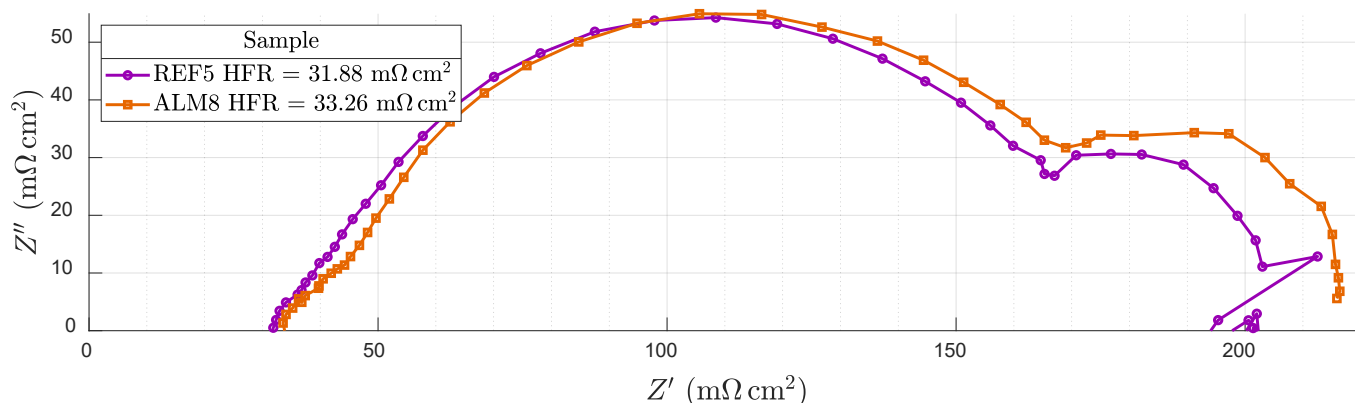
Figure 42 Example Nyquist plot comparing the reference (REF5) and Additive-Layer Manufactured (ALM8) MEA at 0.5 A/cm² measured from 0.02-150 kHz.

The Nyquist plot shows not only membrane resistance but also the polarization resistance. The intercepts at lower frequency on the right side of each graph in Figure 42 are both slightly over 200 mΩ·cm², meaning less variation in catalytic activity.

Table 5 Example High-Frequency Resistance (HFR) from EIS

Sample	Cell resistance (mΩ·cm²)
BENCHMARK*	52.0
REFERENCE MEA	35.48 ± 3.83
ALM MEA	41.62 ± 7.09

* Internal benchmark tested at 21 °C and 50 % RH

ASSESSMENT

Looking at the cell resistance in Table 5, all values are lower than benchmark, cell resistance is prone to change with operation conditions. The proton conductivity of membrane can be simply defined through this analysis. The comparison between ALM and reference shows comparable values when cell was operating at 0.5 A/cm², hence the membrane resistance of ALM CCMs is competitive. EIS can be sped up by applying multi-sine waveform and analysing the data, or performing the measurement at a single frequency predetermined for a given CCM (empty marker corresponds to single-frequency HFR rather than EIS).

Figure 43 Usability of electrochemical impedance spectroscopy for layer characterisation. Filled marker indicates the lab-scale and the empty marker the fab-scale usability, respectively.

2.4.2.5. Cell performance

Following the protocol of internal benchmark testing, conditioning was always conducted before a polarization curve was drawn. The operating parameters were set to the empirical conditions of different fuel cell applications. At cell temperature of 50 °C, ambient pressure on both electrodes with dry anode and 30 %RH cathode is chosen as comparison between cases. The measurement results are shown in Figure 48 and Table 6, a comparison to the internal benchmark value.
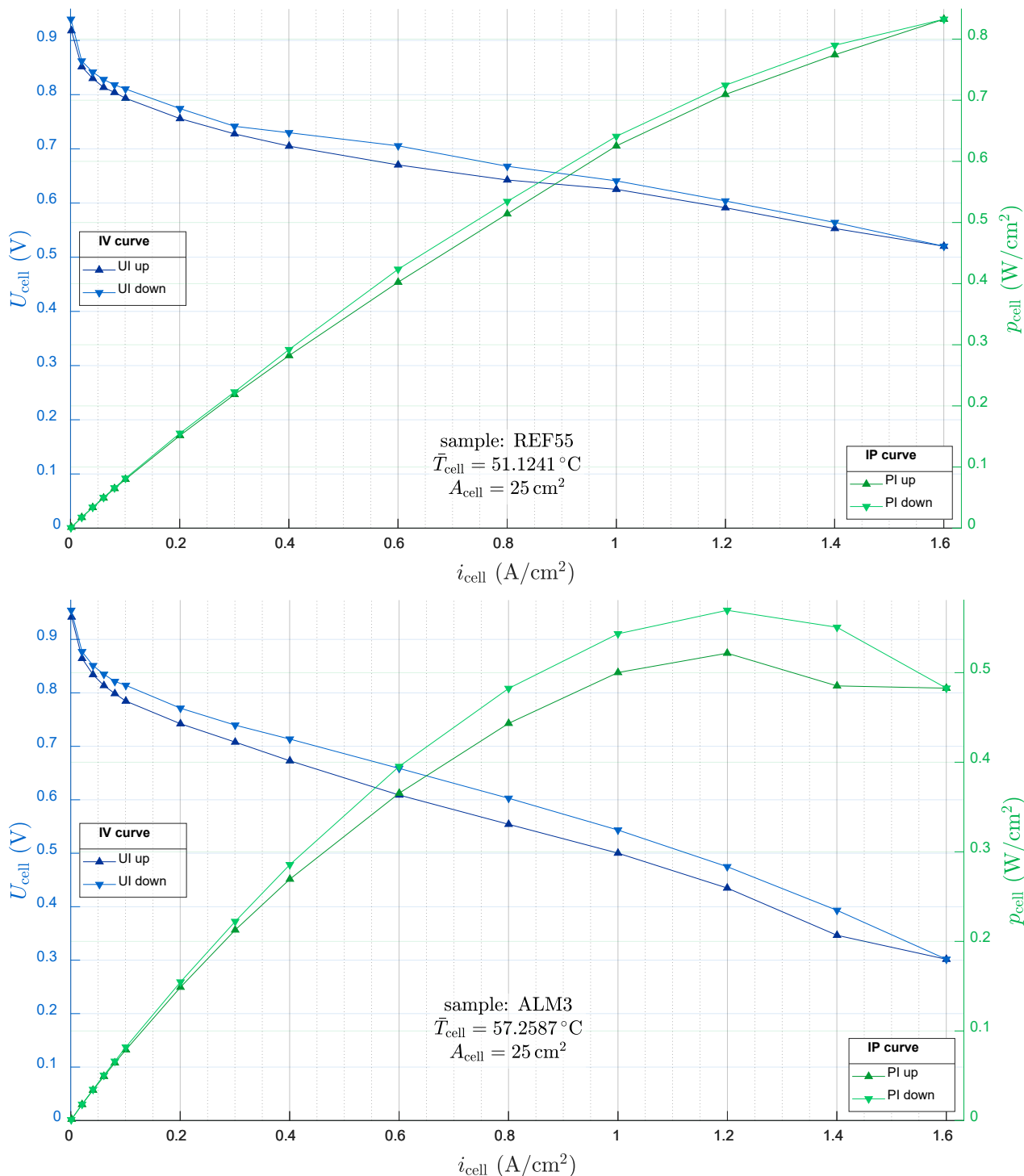
Figure 44 Example Polarisation and power curves of reference MEA (top) and ALM MEA (bottom).

Polarization curves recorded from low-to-high current density and from high-to-low current density are shown in Figure 44. The performance of descending current is higher than ascending current, possibly due to the humidity accumulated when operating at the high current density. The curve separation is more pronounced in the case of the ALM MEA. This could indicate that ALM MEA is more sensitive to humidity changes. It should be noted that the values for ALM MEA in Table 6 summarise five samples (two measured with the original balticFuelCell flow field and three with the new alternative flow field). Samples measured in the modified configuration exhibit the same OCV and voltage at 0.5 A/cm^2, but the peak power increases to $p_{\max} = 805.74 \pm 81.83$ mW/cm^2. The increase in peak power again hints at issues with anode flooding experienced with the original flow field.

Table 6 Cell performance at 50 °C, ambient pressure, dry anode, 30 %RH cathode

Cell performance	OCV (V)	U (V) @ 0.5 A/cm^2	p$_{max}$ (mW/cm^2)
BENCHMARK*	n/a	0.70	816
REFERENCE MEA	0.94 ± 0.01	0.67 ± 0.01	779.08 ± 30.72
ALM MEA	0.95 ± 0.01	0.65 ± 0.02	687.74 ± 171.76

* Internal benchmark provided by JMFC

** modified protocol with vertical orientation

ASSESSMENT

In the last part, the overview of cell performance is summarised in Table 6. Due to the potential effect of flow fields at high current density, the peak power density of ALM did not reach the KPI value of 0.67 W/cm^2. However, cell performance can be further examined by other features of polarization curves such as OCV or cell voltage at a certain current density which can give the information both on catalytic activity and cell resistance. If one looks into the measurements of OCV and cell voltage at 0.5 A/cm^2, the values of ALM-MEAs are in line with the reference, in other words, the ALM CCMs performed at the same level as reference CCMs regardless of factors like flooding, flow configuration, flow field design, etc.

Overall, each of evaluation methods presented above is able to verify the functionality of ALM CCM in different aspects and to be implemented for cross-examination. Furthermore, by applying these evaluation tools it is possible to discover defects and weaknesses of the manufactured MEAs and suggest in future improvements. For the next steps, incorporation of seal materials and achievement of peak power density as per the respective KPI will be investigated in other work packages.

Figure 45 Usability of Functional Layer Characterisation for CCM development. Filled marker indicates the lab-scale and the empty marker the fab-scale usability, respectively.

2.4.3. MECHANICAL TESTING

Along with the electrochemical tests, characterisation of the mechanical properties has been carried out. The tensile strength testing, which defines the mechanical properties of membrane, was performed to compare the intrinsic properties of ALM-made membranes with the state-of-the-art membranes as reference.

2.4.3.1. TENSILE STRENGTH

An in-house developed equipment was built for the characterisation of mechanical properties of deposited layers by mechanical stress tests of fuel cell materials and components. Relevant temperature and humidity are facilitated by a climate chamber CTC256 by Memmert (Figure 46) housing the tensile test equipment with specimen samples (Figure 47).

Figure 46 Customized tensile testing platform. (source: TUC)

Here we summarize the measurements of CCMs made by the conventional method and ALM method in parallel to the internal benchmark in Table 7, stress-strain curves in Figure 48. It should be noted that the conditions used for benchmark differ from those used for the tests here. We chose 20 °C/80 %RH and 80 °C/80 %RH to have a reasonable approximation of real operating conditions for fuel cells.
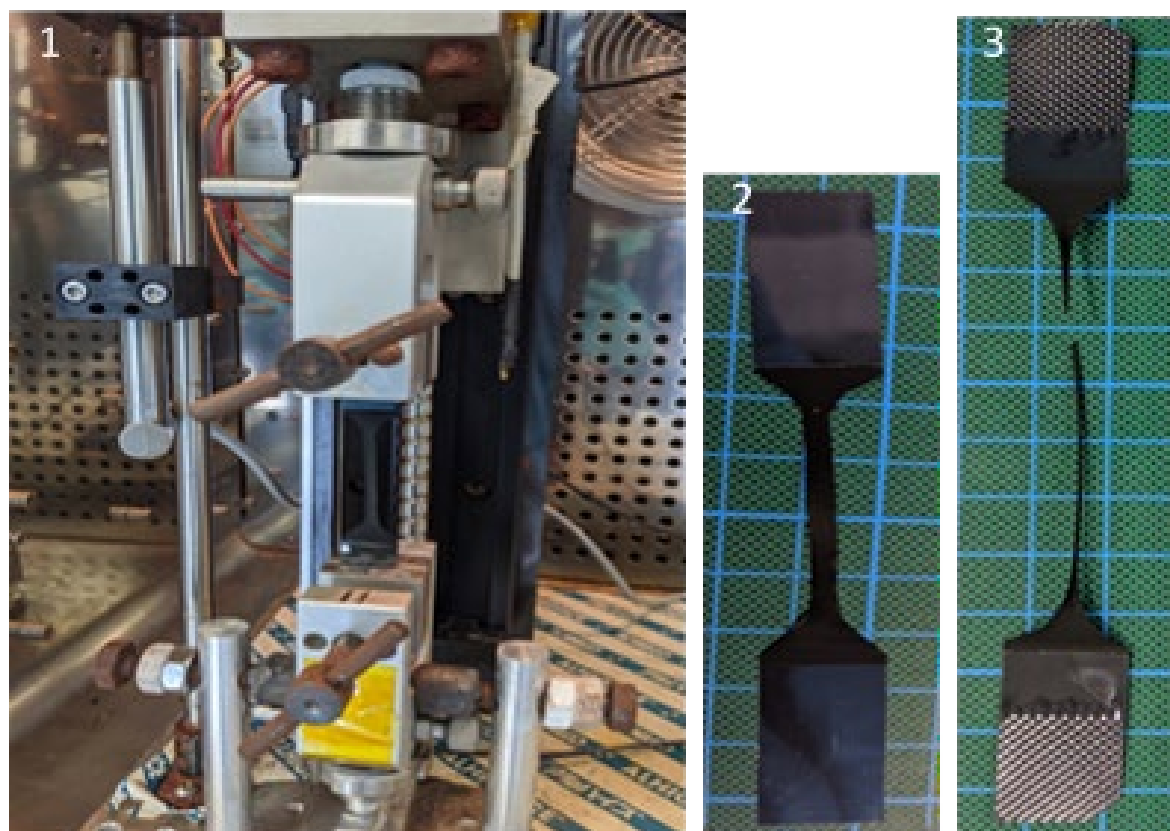
Figure 47 1. Tensile testing equipment in climate chamber with sample clamped on the grips. 2. CCM sample before test. 3. CCM sample after test. (source: TUC)

At 20 °C, the material was mostly under elastic deformation before reaching the ultimate strength, meanwhile at 80 °C, the material underwent a longer process of thinning before elongation at break. The measurements done at 80 °C provided a broad range of results implied by the wide uncertainties as apparent from Table 7.

Table 7 Characterization of mechanical properties of membrane/CCM

Tensile testing	Ultimate tensile strength (MPa)	Tensile modulus (MPa)	Elongation at break (%)
21℃, 50%RH			
BENCHMARK*	25.00-30.00	n/a	120.00
20℃, 80%RH			
REFERENCE MEA	14.24 ± 1.32	78.76 ± 15.28	90.45 ± 5.55
ALM MEA	15.88 ± 1.12	99.66 ± 11.42	90.85 ± 11.42
80℃, 80%RH			
REFERENCE MEA	6.05 ± 0.38	46.03 ± 15.54	70.64 ± 39.69
ALM MEA	7.35 ± 0.34	25.79 ± 1.89	128.00 ± 13.92

* Internal benchmark (here a standalone membrane) provided by JMFC
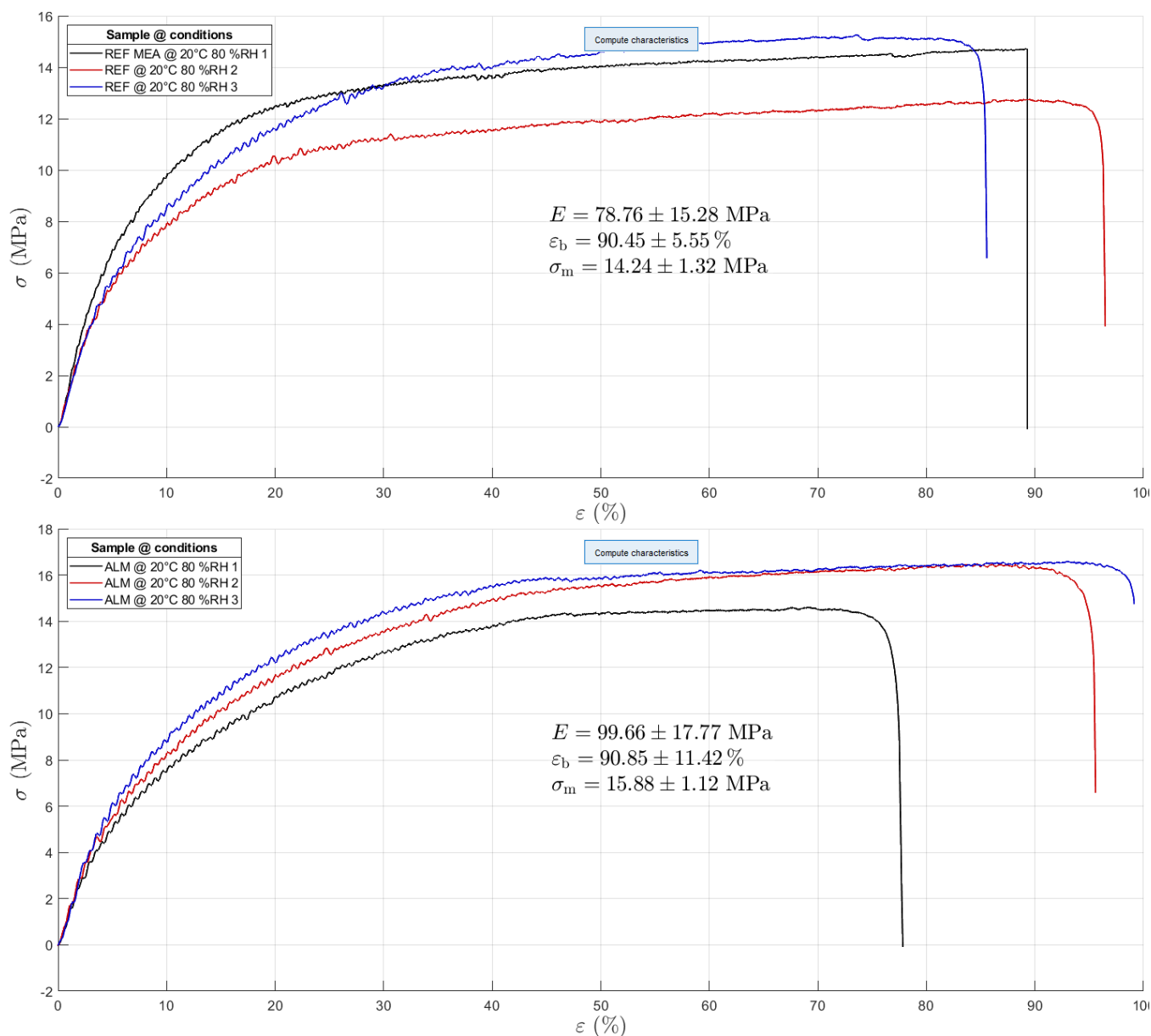
Figure 48 Example stress-strain curves of reference MEA (left) and ALM MEA (right); at 20℃, 80 %RH.

In Figure 48 (top/bottom right), the curves for reference and ALM CCMs exhibit comparable properties. The difference when compared to benchmark can be partly attributed to the increased relative humidity, which weakens the tested materials.

2.4.3.2. ASSESSMENT

The mechanical properties of membrane measured by tensile testing inTable 7 show that the ultimate tensile strength of ALM and reference CCMs are all lower than benchmark. Tensile strength is significantly affected by ambient conditions; therefore, using customized test bench with climate chamber provides valuable simulated characteristics of utilised materials under relevant operating conditions. Tensile strength, tensile modulus and elongation at break were chosen to assess the robustness, flexibility and ductility of materials in question. The variation between reference and ALM is apparent from the results. Other mechanical properties can also be inferred from the stress-strain curve. It should be noted that both reference and ALM samples could not demonstrate the same

elongation performance as benchmark, possibly due to the difference in the test parameters and specimen preparation.

Figure 49 Usability of Functional Layer Characterisation for CCM development. Filled marker indicates the lab-scale and the empty marker the fab-scale usability, respectively.

2.5. ACCELERATED STRESS TEST – AST

Accelerated stress tests are a tool to assess material durability in a reduced amount of time as compared to real life operation by triggering specific degradation modes that are either expected due to the target application or known material characteristics. This becomes ever more crucial with the extended lifetime expectations of state of the art and beyond MEA materials of 20,000 h and more. A suite of ASTs was presented in detail elsewhere (D3.2 and D5.2) and will not be repeated here in sake of brevity.

3. CONCLUSIONS

This deliverable report describes characterisation tools and procedures used within MAMA-MEA for deposited layers and their properties. The testing procedures and equipment are described and accompanied with the test results and their interpretation. Formulation of inks (2.1), visual methods (2.2.1, 2.2), morphology (chapter 2.1), functional layer characterisation (2.4) up to AST (2.5). Depending on the desired target, an applicable set of technologies out of these can be selected from the presented range.

4. REFERENCES

1. https://www.triumphadler.de. [Online] [Cited: 30 03 2020.]
2. Veeco Instruments Inc. *Broschure "Dektak 150 Surface Profiler"*. 2006.
3. MAMA-MEA, Deliverable 5.1. *Report on suitable test protocols and baseline testing.*